

Bayesian Bridge Gaussian Process Regression

Minshen Xu ^a, Shiwei Lan ^b, Lulu Kang ^a

^a Department of Mathematics and Statistics,
University of Massachusetts Amherst, Amherst, MA, United States
^b School of Mathematical and Statistical Sciences,
Arizona State University, Tempe, AZ, United States

Abstract

The performance of Gaussian Process (GP) regression is often hampered by the curse of dimensionality, which inflates computational cost and reduces predictive power in high-dimensional problems. Variable selection is thus crucial for building efficient and accurate GP models. Inspired by Bayesian bridge regression, we propose the Bayesian Bridge Gaussian Process Regression (B²GPR) model. This framework places ℓ_q -norm constraints on key GP parameters to automatically induce sparsity and identify active variables. We formulate two distinct versions: one for $q = 2$ using conjugate Gaussian priors, and another for $0 < q < 2$ that employs constrained flat priors, leading to non-standard, norm-constrained posterior distributions. To enable posterior inference, we design a Gibbs sampling algorithm that integrates Spherical Hamiltonian Monte Carlo (SphHMC) to efficiently sample from the constrained posteriors when $0 < q < 2$. Simulations and a real-data application confirm that B²GPR offers superior variable selection and prediction compared to alternative approaches.

Keywords: Bayesian Bridge Regression; Gaussian Process; Gibbs Sampling; Hamiltonian Monte Carlo; Regularization; Spherical Hamiltonian Monte Carlo.

1 Introduction

Gaussian Process (GP) regression is a widely used statistical method for modeling complex nonlinear relationships, particularly in computer experiments and simulations. However, it faces the curse of dimensionality due to a high-dimensional input space, resulting in high computational demands and diminished predictive performance. In practice, many simulation models primarily depend on a small subset of influential inputs. Identifying these key variables is critical for enhancing the efficiency and accuracy of GP regression.

1.1 Related Literature

Regularization methods are essential tools for preventing overfitting and identifying significant predictors in linear and generalized linear models. For the linear regression model $Y(\mathbf{x}) = \mathbf{x}^\top \boldsymbol{\beta} + \epsilon$, frequentist regularization approaches introduce penalty terms to constrain the coefficients $\boldsymbol{\beta}$. Ridge regression (Hoerl and Kennard, 1970) employs an l_2 -norm

penalty, which shrinks coefficients uniformly without performing variable selection. In contrast, LASSO by [Tibshirani \(1996\)](#) uses an l_1 -norm penalty to induce sparsity by driving some coefficients to zero, thereby enabling variable selection. The Elastic Net ([Zou and Hastie, 2005](#)) combines l_1 and l_2 penalties, offering a balance between shrinkage and selection, which is particularly useful in high-dimensional settings where the number of predictors exceeds the number of observations. Bridge regression ([Frank and Friedman, 1993](#)) generalizes these methods with a flexible ℓ_q -norm penalty ($q \geq 0$), allowing adaptive control over both shrinkage intensity and selection behavior.

While closed-form solutions for arbitrary q were not derived, the authors highlighted the importance of optimizing q based on the data.

Bayesian regularization methods consider these penalties as prior distributions, updating them with observed data to obtain posterior estimates. Bayesian ridge regression by [Bishop \(2006\)](#) assigns Gaussian priors to coefficients, yielding posteriors whose mode aligns with the l_2 -penalized estimates from the frequentist ridge regression. Similarly, [Park and Casella \(2008\)](#) proposed the Bayesian LASSO that adopts the Laplace prior distribution, replicating the sparsity-inducing properties of the l_1 penalty. For more flexible regularization, Bayesian bridge regression ([Polson et al., 2014](#)) employs priors analogous to the ℓ_q penalty, enabling adaptive shrinkage and selection. While Bayesian methods often involve computationally intensive Markov Chain Monte Carlo (MCMC) sampling, they provide a natural framework for uncertainty quantification, unlike their frequentist counterparts, which rely on convex optimization.

In GP modeling, regularization techniques have been adapted to address the challenges of the curse of dimensionality. Frequentist approaches include penalized blind kriging ([Hung, 2011](#)) that introduces penalties on the regression coefficients of the mean function of the GP, and methods like [Li and Sudjianto \(2005\)](#) that impose penalties directly on covariance hyperparameters. Bayesian GP methods, on the other hand, often employ threshold or indicator-based variable selection. For instance, [Hu and Dey \(2024\)](#) identified active variables by thresholding on the samples from the posterior of the inverse length-scale hyperparameters of the correlation function, while [Zhang et al. \(2023\)](#) proposed to use an indicator to decide if an input variable is significant or not. In their framework, an input variable is deemed to be active if its corresponding parameters are significant in either the mean function or the covariance function.

1.2 Our Contribution

The aforementioned regularization methods for GP models reveal the trade-off between computational tractability and modeling flexibility, and they motivate our proposed *Bayesian Bridge Gaussian Process Regression (B²GPR)* framework. It integrates the adaptive shrinkage property of the Bridge regression with the probabilistic foundations of Gaussian Processes. Unlike [Hung \(2011\)](#) and [Li and Sudjianto \(2005\)](#), our method simultaneously regularizes both the mean function's regression coefficients and the covariance function's hyperparameters through the flexible ℓ_q penalty. While initially conceptualized within a frequentist penalized optimization framework, we identified two critical challenges: (1) the non-convexity of the optimization landscape, and (2) the computational burden of gradient evaluations for covariance hyperparameters under the ℓ_q -norm constraints.

To resolve these limitations, we reformulate the problem within the Bayesian framework, extending the Bayesian bridge regression to the GP context. This transition introduces a

challenge—particularly in constructing appropriate prior distributions that enforce ℓ_q -norm constraints on GP parameters. The traditional exponential-power prior for Bayesian bridge regression does not work for the covariance hyperparameters, as it loses the scale mixture representations of the posterior, which enable easy Gibbs sampling. We address this by adopting the truncated prior distributions that lead to constrained posterior distributions. This construction ensures the mode of the posterior distributions of the parameters exactly corresponds to the estimates of the regularized loss function in the frequentist approach.

However, sampling from the constrained posterior distribution requires special techniques. The Spherical Hamiltonian Monte Carlo (SphHMC) method (Lan et al., 2014), originally designed for spherical constraint spaces, provides a suitable solution to our problem. We use the SphHMC to sample the parameters of the mean and the correlation function and integrate it into the overall Gibbs sampling framework for all the parameters when ℓ_q -norm with $0 < q < 2$ is used. This constrained MCMC procedure enables efficient exploration of the posterior distribution. It shows three main advantages: (1) flexibility of the choice in prior distributions; (2) variable selection through the ℓ_q penalty; (3) accurate prediction. For $q = 2$, Gaussian prior distributions on the parameters naturally correspond to the l_2 -norm penalty, and thus we only need to use a conventional sampling approach. Here, we use Hamiltonian Monte Carlo for the $q = 2$ case.

Compared to the frequentist regularization approach, Bayesian framework has the advantage of fully exploring the multimodal posterior distribution in the high-dimensional space, which returns more accurate estimates and predictions than the single point estimates as in the frequentist methods. More importantly, statistical inferences are possible based on the posterior samples for all parameters, including hyperparameters. Unfortunately, frequentist methods only return single point estimates without any inferences. More importantly, the frequentist methods choose tuning parameter for the regularization term using cross-validation. This is far more computational than the Bayesian framework in which we combine the sampling of all the tuning parameters with other parameters in full Bayes fashion and proves to be more efficient.

The paper proceeds as follows. Section 2 establishes the theoretical basis, reviewing GP models and bridge regularization in both frequentist and Bayesian settings. Section 3 introduces the B²GPR model, formalizing the generalized bridge prior and its frequentist-Bayesian duality. Section 4 details our computational methods, presenting the modified SphHMC algorithm for constrained posterior sampling. Sections 5 and 6 validate the method through simulated experiments and a real-case study, demonstrating superior performance in variable selection and prediction accuracy. We conclude with discussion and future directions in Section 7.

2 Preliminaries

2.1 Gaussian Process model

A Gaussian Process (GP) is a stochastic process characterized by the property that any finite collection of the function values, evaluated at different input locations, follows a multivariate normal distribution. We can fully specify a GP by the mean and covariance function. Given the input domain $\Omega \subset \mathbb{R}^d$, we focus on the univariate GP. Specially, we

assume the random process $Y(\mathbf{x}) \in \mathbb{R}^1$ at any input point $\mathbf{x} \in \Omega$ is

$$Y(\mathbf{x}) = \underbrace{\mathbf{g}(\mathbf{x})^\top \boldsymbol{\beta}}_{\text{fixed effect}} + \underbrace{Z(\mathbf{x})}_{\text{random effect}} + \underbrace{\epsilon}_{\text{noise}}. \quad (1)$$

In the fixed effect term, $\mathbf{g}(\mathbf{x})$ is a p -dimensional vector of user-specified basis functions. Often we use polynomial functions of \mathbf{x} up to a chosen degree. For instance, a two-dimensional quadratic polynomial basis functions are $\mathbf{g}(\mathbf{x}) = [1, x_1, x_2, x_1^2, x_1 x_2, x_2^2]^\top$. Correspondingly, $\boldsymbol{\beta}$ is a p -dimensional vector of linear coefficients. The random noise term, $\epsilon \sim \mathcal{N}(0, \sigma^2)$, is independent of all the other model components. The random effect term $Z(\mathbf{x})$ follows a zero-mean stationary Gaussian Process, denoted as $Z(\mathbf{x}) \sim \mathcal{GP}(0, \tau^2 K(\cdot, \cdot; \boldsymbol{\omega}))$, with variance parameter τ^2 and correlation function $K(\cdot, \cdot; \boldsymbol{\omega})$ with hyperparameters $\boldsymbol{\omega}$. The correlation function $K(\cdot, \cdot; \boldsymbol{\omega}) : \Omega \times \Omega \mapsto \mathbb{R}_+$ must be a symmetric, positive definite kernel function. A common choice for the correlation kernel is the separable anisotropic Gaussian kernel,

$$K(\mathbf{x}_i, \mathbf{x}_j; \boldsymbol{\omega}) = \exp \left\{ - \sum_{k=1}^d \omega_k^2 (x_{ik} - x_{jk})^2 \right\},$$

with the correlation hyperparameters $\boldsymbol{\omega} \in \mathbb{R}^d$ which control the shape of the kernel functions. They have been referred to as *correlation strength* or *inverse length-scale* hyperparameters in the literature.

Under the model assumption, given the parameters $\boldsymbol{\theta} = (\boldsymbol{\beta}, \boldsymbol{\omega}, \tau^2, \eta)$, where $\eta = \sigma^2 / \tau^2$, $Y(\mathbf{x})$ is a GP with mean and covariance as follows:

$$\begin{aligned} \mathbb{E}[Y(\mathbf{x})] &= \mathbf{g}(\mathbf{x})^\top \boldsymbol{\beta}, \quad \forall \mathbf{x} \in \Omega \\ \text{cov}[Y(\mathbf{x}_i), Y(\mathbf{x}_j)] &= \tau^2 K(\mathbf{x}_i, \mathbf{x}_j; \boldsymbol{\omega}) + \sigma^2 \delta(\mathbf{x}_i, \mathbf{x}_j), \quad \forall \mathbf{x}_i, \mathbf{x}_j \in \Omega, \\ &= \tau^2 [K(\mathbf{x}_i, \mathbf{x}_j; \boldsymbol{\omega}) + \eta \delta(\mathbf{x}_i, \mathbf{x}_j)], \end{aligned}$$

where $\delta(\mathbf{x}_i, \mathbf{x}_j) = 1$ if $\mathbf{x}_i = \mathbf{x}_j$ and 0 otherwise. Denote the observed data from a certain computer or physical experiment by $\{\mathbf{x}_i, y_i\}_{i=1}^n$, the set of n design points by $\mathcal{X}_n = \{\mathbf{x}_1, \dots, \mathbf{x}_n\}$, and the response data by $\mathbf{y} = [y_1, \dots, y_n]^\top$. Given the parameter $\boldsymbol{\theta}$, the posterior predictive distribution of $Y(\mathbf{x})$ at any query point \mathbf{x} is the following normal distribution

$$Y(\mathbf{x}) | \mathbf{y}, \boldsymbol{\theta} \sim \mathcal{N}(\mu_n(\mathbf{x}), \sigma_{\mathbf{x}|n}^2),$$

where

$$\begin{aligned} \mu_n(\mathbf{x}) &= \mathbb{E}(Y(\mathbf{x}) | \mathbf{y}, \boldsymbol{\theta}) = \mathbf{g}(\mathbf{x})^\top \boldsymbol{\beta} + \mathbf{k}(\mathbf{x})^\top (\mathbf{K} + \eta \mathbf{I}_n)^{-1} (\mathbf{y} - \mathbf{G}\boldsymbol{\beta}), \\ \sigma_{\mathbf{x}|n}^2(\mathbf{x}) &= \tau^2 \left\{ 1 - \mathbf{k}(\mathbf{x})^\top (\mathbf{K} + \eta \mathbf{I}_n)^{-1} \mathbf{k}(\mathbf{x}) \right\}, \\ \mathbf{k}(\mathbf{x}) &= K(\mathbf{x}, \mathcal{X}_n) = K(\mathcal{X}_n, \mathbf{x}) = [K(\mathbf{x}, \mathbf{x}_1), \dots, K(\mathbf{x}, \mathbf{x}_n)]^\top \end{aligned}$$

The derivations can be found in [Santner et al. \(2003\)](#) and [Williams and Rasmussen \(2006\)](#).

For physical or stochastic computer experiments, σ^2 is typically estimated by the pooled variance from replications if there are replicated observations at some design points. For deterministic computer experiments, since there is no measurement noise involved, σ^2 should be specified as 0, and thus $\eta = 0$. In this case, the posterior predictive mean $\mu_n(\mathbf{x})$ interpolates all the training data. However, it is usually advantageous to specify a small

positive value for η known as the *nugget* value (Peng and Wu, 2014) to overcome the possible ill-conditioning of the kernel matrix \mathbf{K} . In this paper, the estimation and inference of the unknown parameters $\boldsymbol{\theta}$ and prediction inference are conducted under the Bayesian framework.

2.2 Bayesian Bridge Regression

Bayesian Bridge regression is a Bayesian approach that achieves bridge regularization for regression models. Consider a linear regression model defined by $\mathbf{y} = \mathbf{X}\boldsymbol{\beta} + \boldsymbol{\epsilon}$ for data $\{\mathbf{x}_i, y_i\}_{i=1}^n$ with the error term $\boldsymbol{\epsilon} \sim \mathcal{MVN}_n(\mathbf{0}, \sigma^2 \mathbf{I}_n)$. The bridge regression, introduced by Frank and Friedman (1993), estimates coefficients $\boldsymbol{\beta}$ by solving the following minimization problem:

$$\min_{\boldsymbol{\beta}} \frac{1}{2} \|\mathbf{y} - \mathbf{X}\boldsymbol{\beta}\|_2^2 + \lambda \sum_{j=1}^p |\beta_j|^q, \quad (2)$$

where \mathbf{y} is the $n \times 1$ response vector, \mathbf{X} is the $n \times p$ matrix of regressors, and $\boldsymbol{\beta}$ is the $p \times 1$ vector of regression coefficients to be estimated. The tuning parameter $\lambda > 0$ controls the strength of penalization, and the parameter $q \geq 0$ adjusts the shape of the penalty (Mallick and Yi, 2018). Notably, when $q = 0$ (with the convention $0^0 = 0$), the penalty corresponds to the number of nonzero coefficients, resembling the best subset selection. Other special cases include LASSO regression (Tibshirani, 1996) with $q = 1$ and ridge regression (Hoerl and Kennard, 1970) with $q = 2$. Thus, bridge regression generalizes these methods into a unified framework. It bridges a class of shrinkage and selection operators, allowing for flexible regularization and variable selection.

For the penalty term, we can also write it as $\lambda \|\boldsymbol{\beta}\|_q$, where $\|\cdot\|_q$ is the ℓ_q -norm of a vector. Based on Hastie et al. (2009), bridge regression problem (2) can be equivalently expressed as a constrained minimization problem:

$$\min_{\boldsymbol{\beta}} \frac{1}{2} \|\mathbf{y} - \mathbf{X}\boldsymbol{\beta}\|_2^2 \quad \text{subject to} \quad \|\boldsymbol{\beta}\|_q = \left(\sum_{j=1}^p \beta_j^q \right)^{1/q} \leq t. \quad (3)$$

This explicitly imposes a size constraint on the coefficients $\boldsymbol{\beta}$, establishing a direct one-to-one correspondence between the penalty parameter λ and the constraint t . The constraint is concave when $0 < q < 1$ and convex when $q \geq 1$.

The above is the frequentist formulation. From the Bayesian perspective, bridge regression naturally corresponds to specifying a particular prior distribution for the regression coefficients. Following the penalization form in (2), Park and Casella (2008) and Polson et al. (2014) introduced the exponential-power prior distribution for $\boldsymbol{\beta}$ given λ

$$p(\boldsymbol{\beta}|\lambda) \propto \prod_{j=1}^p \exp(-\lambda|\beta_j|^q). \quad (4)$$

This prior is the Laplace distribution when $q = 1$ and the Gaussian distribution when $q = 2$. Combining with the prior distribution of λ , the joint prior of all parameters has a mixture representation which enables efficient Gibbs sampling of the posterior distribution. It is one of the key advantages of the Bayesian bridge approach.

Alternative to the exponential-power prior, the constrained formulation (3) leads to a constrained prior distribution for β (omitting the normalizing constant):

$$p(\beta|t) \propto p(\beta)\mathbb{I}(\|\beta\|_q \leq t),$$

and it leads to the posterior distribution for β

$$p(\beta|y, t) \propto p(y|\beta)p(\beta)\mathbb{I}(\|\beta\|_q \leq t).$$

Here \mathbb{I} is an indicator function, and it is equal to one if the input statement is true and zero otherwise. The posterior mode can be obtained by minimizing $-\log p(\beta|y, t)$, which is equal to minimizing $-\log p(y|\beta) - \log p(\beta)$ subject to $\|\beta\|_q \leq t$. Hence, if using the non-informative prior for β , finding the posterior mode is equivalent to solving the frequentist constrained optimization problem (3). However, this constrained prior is not restrictive to non-informative priors. It offers greater flexibility by allowing a wide variety of alternative distributions that encode additional information or preferences about the predictors.

3 Bayesian Bridge Gaussian Proces Regression

Extending the Bridge regression concept to the GP model described in (1), we introduce a regularization strategy that penalizes both the linear coefficients β and the correlation parameters ω . Under the frequentist framework, to estimate the unknown parameters of the penalized GP regression is to solve the minimization problem

$$\min_{\beta, \omega} \left\{ -\log p(y|\beta, \omega, \tau^2, \eta) + \lambda_1 \sum_{j=1}^p |\beta_j|^q + \lambda_2 \sum_{j=1}^d |\omega_j|^q \right\}, \quad (5)$$

where $-\log p(y|\beta, \omega, \tau^2, \eta)$ is the negative log-likelihood function, and the two regularization terms represent the ℓ_q -norm penalties on the parameters (β, ω) , controlling shrinkage intensity through tuning parameters λ_1 and λ_2 . Given (β, ω, η) , the parameter τ^2 can be estimated via maximum likelihood estimation. The nugget effect η can be computed as a tuning parameter via cross-validation or through optimization. The overall estimation of all $(\beta, \omega, \tau^2, \eta)$ can take iterative steps by separately computing (β, ω) , τ^2 , and η . We call it *Bridge Gaussian Process Regression* with $0 < q \leq 2$.

Just like the equivalency between (2) and (3), (5) is equivalent to the constrained minimization problem:

$$\min_{\beta, \omega} \{-\log p(y|\beta, \omega, \tau^2, \eta)\} \quad \text{subject to} \quad \|\beta\|_q \leq r_\beta, \quad \|\omega\|_q \leq r_\omega. \quad (6)$$

This formulation explicitly introduces constraints on ℓ_q -norm of β and ω . There is also an one-to-one correspondence between penalty parameters (λ_1, λ_2) and constraints (r_β, r_ω) .

Given that y still follows a multivariate normal distribution, the exponential-power prior for β can still lead to a mixture representation of the conditional posterior for β , enabling fast Gibbs sampling. Unfortunately, this idea does not work for ω . Rather, we choose the more flexible formulation (6). The bridge constraints in (6) can be implemented through truncated prior distributions, i.e.,

$$\beta \sim p(\beta)\mathbb{I}(\|\beta\|_q \leq r_\beta) \quad \text{and} \quad \omega \sim p(\omega)\mathbb{I}(\|\omega\|_q \leq r_\omega),$$

omitting the normalizing constants. Based on the truncated prior distributions, the conditional posterior distributions for β and ω are

$$\begin{aligned} p(\beta|\mathbf{y}, \omega, \tau^2, \eta, r_\beta) &\propto p(\mathbf{y}|\beta, \omega, \tau^2, \eta)p(\beta)\mathbb{I}(\|\beta\|_q \leq r_\beta), \\ p(\omega|\mathbf{y}, \beta, \tau^2, \eta, r_\omega) &\propto p(\mathbf{y}|\beta, \omega, \tau^2, \eta)p(\omega)\mathbb{I}(\|\omega\|_q \leq r_\omega). \end{aligned}$$

To find the posterior modes of β and ω , we just need to solve the following two minimization problems.

$$\begin{aligned} \min_{\beta} -\log p(\mathbf{y}|\beta, \omega, \tau^2, \eta) - \log p(\beta) &\quad \text{s.t. } \|\beta\|_q \leq r_\beta, \\ \min_{\omega} -\log p(\mathbf{y}|\beta, \omega, \tau^2, \eta) - \log p(\omega) &\quad \text{s.t. } \|\omega\|_q \leq r_\omega. \end{aligned} \tag{7}$$

As discussed on Bayesian bridge regression, if non-informative priors are used, i.e., $p(\beta) \propto 1$ and $p(\omega) \propto 1$, (7) and (6) are the same, with the minor difference that (6) jointly computes β and ω whereas (7) computes one given the other. Other than the non-informative priors, we can use any other suitable alternatives, such as normal distributions, for β and ω for more flexibility. However, in that case, there is a redundancy in regularization. The normal prior distributions have applied the l_2 -norm regularization on (β, ω) , but the constraints would apply l_q -norm regularization again.

In the next section, we introduce two versions of the B²GR.

1. For $0 < q < 2$, we adopt the non-informative prior distributions for (β, ω) and impose the l_q -norm constraints. To overcome the challenge of sampling from the constrained posterior distributions, we incorporate the Spherical Hamiltonian Monte Carlo within the Gibbs sampling framework. For short, we name this version sph-B²GR.
2. For $q = 2$, we adopt informative Gaussian distributions for (β, ω) . But to avoid the redundancy of l_2 regularization and l_q -norm constraint, we remove the l_q -norm constraints in this case. The full Bayes framework is developed, and the sampling of (β, ω) is via Hamiltonian Monte Carlo without constraints. For short, we name the second version hmc-B²GR.

As pointed out by [Polson et al. \(2014\)](#), both the frequentist and Bayesian approaches for the GP regression face the same practical challenge: exploring and summarizing the multimodal likelihood or posterior distribution in the high-dimensional Euclidean space. [Polson et al. \(2014\)](#) made several compelling arguments in favor of the fully Bayesian approach, many of which apply to our setting. First, it is misleading to summarize a multimodal surface via a single point estimate, and the MCMC sampling approach is more effective at exploring the entire likelihood surface. Second, statistical inference is possible for all the hyperparameters based on the posterior sampling. Third, the frequentist approach chooses the tuning parameter (r_β, r_ω) via cross-validation, which is computational demanding and lacks uncertainty quantification. In the Bayesian approach, sph-B²GR, we assume non-informative priors on (r_β, r_ω) and sample their values from their respective conditional posterior distribution. Compared to cross-validation, which has to estimate all parameters for each pair of possible (r_β, r_ω) , the full Bayes approach combines the sampling of (r_β, r_ω) with other parameters and proves to be more efficient. Similarly, for hmc-B²GR, the regularization is applied through the variance parameters of the prior distribution, which are also incorporated in the MCMC sampling of the posterior distributions.

Compared to Bayesian bridge regression, the sampling procedure for B²GPR is more difficult since the computation for the correlation parameters and nugget effect is more time-consuming due to the inverse of the $n \times n$ covariance matrix in each iteration. Therefore, we develop the MCMC sampling procedure based on the Hamiltonian Monte Carlo, which is more efficient compared to conventional Metropolis-Hastings type of algorithms.

4 Posterior Sampling

4.1 HMC and Spherical HMC

Hamiltonian Monte Carlo (HMC) (Neal, 2011) is an MCMC method that leverages Hamiltonian dynamics to efficiently explore complex target distributions. The sampler operates on an augmented state space of position parameters $\boldsymbol{\theta}$ and momentum variables $\boldsymbol{\phi} \sim \mathcal{N}(\mathbf{0}, \mathbf{M})$. The system's evolution is governed by the Hamiltonian $H(\boldsymbol{\theta}, \boldsymbol{\phi}) = U(\boldsymbol{\theta}) + K(\boldsymbol{\phi})$, where $U(\boldsymbol{\theta}) = -\log p(\boldsymbol{\theta})$ is the potential energy and $K(\boldsymbol{\phi}) = \frac{1}{2} \boldsymbol{\phi}^\top \mathbf{M}^{-1} \boldsymbol{\phi}$ is the kinetic energy. Numerical simulation via the leapfrog integrator (Algorithm S1) generates distant, high-acceptance proposals, enabling efficient sampling from high-dimensional posteriors.

While HMC is powerful, it does not inherently handle parameter constraints. Spherical HMC (SphHMC) (Lan et al., 2014; Lan and Shahbaba, 2016) addresses this for norm-constrained domains. The core idea is *spherical augmentation*. The domain defined by the ℓ_q -norm constraint on the parameter is $\boldsymbol{\beta} \in \mathbb{R}^d$ as $\mathcal{Q}^d := \{\boldsymbol{\beta} \in \mathbb{R}^d \mid \|\boldsymbol{\beta}\|_q \leq 1\}$, without loss of generality. It can be bijectively mapped to the d -dimensional unit ball, $\mathcal{B}_0^d(1) = \{\boldsymbol{\theta} \in \mathbb{R}^d \mid \|\boldsymbol{\theta}\|_2 \leq 1\}$, by either $\beta_i \mapsto \theta_i = \text{sgn}(\beta_i)|\beta_i|^{q/2}$ or $\boldsymbol{\beta} \mapsto \boldsymbol{\theta} = \boldsymbol{\beta} \frac{\|\boldsymbol{\beta}\|_\infty}{\|\boldsymbol{\beta}\|_2}$. Then it is embedded onto a sphere \mathcal{S}^d in \mathbb{R}^{d+1} by adding $\theta_{d+1} = \pm \sqrt{1 - \|\boldsymbol{\theta}\|_2^2}$. This transforms the boundary into the sphere's equator, allowing the sampler (Algorithm S2) to move freely on \mathcal{S}^d while implicitly respecting the original constraints. We invite readers to go to the Supplement for more in depth review and the Algorithms S1 and S2.

In this article, we impose the ℓ_q -norm constraints on both $\boldsymbol{\omega}$ and $\boldsymbol{\beta}$ as defined in (7) for $0 < q \leq 2$. As explained in the previous section, hmc-B²GPR (for $q = 2$) only needs to use HMC in Algorithm S1, whereas sph-B²GPR (for $0 < q < 2$) calls the spherical HMC in Algorithm S2 to deal with the norm constraint. In sph-B²GPR, the bijectively map from the ℓ_q norm constraints $\|\boldsymbol{\beta}\|_q \leq r_\beta$ and $\|\boldsymbol{\omega}\|_q \leq r_\omega$ are

$$\beta_i \mapsto \theta_{\beta_i} = \text{sgn}(\beta_i) \left| \frac{\beta_i}{r_\beta} \right|^{q/2}, \quad \omega_i \mapsto \theta_{\omega_i} = \text{sgn}(\omega_i) \left| \frac{\omega_i}{r_\omega} \right|^{q/2}.$$

We sample the auxiliary variables $\boldsymbol{\theta}_\beta$ and $\boldsymbol{\theta}_\omega$ from the unit ball using the SphHMC method, and then transform the samples $\boldsymbol{\theta}_\beta$ and $\boldsymbol{\theta}_\omega$ back to the original constrained parameter spaces $\boldsymbol{\beta}$ and $\boldsymbol{\omega}$ using the inverse mappings:

$$\theta_{\beta_i} \mapsto \beta_i = r_\beta \cdot \text{sgn}(\theta_{\beta_i}) |\theta_{\beta_i}|^{2/q}, \quad \theta_{\omega_i} \mapsto \omega_i = r_\omega \cdot \text{sgn}(\theta_{\omega_i}) |\theta_{\omega_i}|^{2/q}.$$

4.2 Sampling for sph-B²GPR

For the sph-B²GPR approach, we use the non-informative prior for $\boldsymbol{\beta}$ and $\boldsymbol{\omega}$, but still need to specify the prior distributions for $(\tau^2, \eta, r_\beta, r_\omega)$. Below is a summary of the prior

distributions for all the parameters.

$$\begin{aligned}
p(\boldsymbol{\beta}|r_\beta) &\propto \mathbb{I}(\|\boldsymbol{\beta}\|_q \leq r_\beta), & \text{constrained non-informative prior,} \\
p(r_\beta) &\propto 1, & \text{non-informative prior,} \\
p(\boldsymbol{\omega}|r_\omega) &\propto \mathbb{I}(\|\boldsymbol{\omega}\|_q \leq r_\omega), & \text{constrained non-informative prior,} \\
p(r_\omega) &\propto 1, & \text{non-informative prior,} \\
\tau^2 &\sim \text{Inverse-}\chi^2(df_{\tau^2}), & \eta \sim \Gamma(a_\eta, b_\eta).
\end{aligned} \tag{8}$$

The hyperparameters $df_{\tau^2}, a_\eta, b_\eta$ are user-specified.

Given data, the sampling distribution is:

$$\mathbf{y}_n|\boldsymbol{\theta} \sim \mathcal{MVN}_n(\mathbf{G}\boldsymbol{\beta}, \tau^2(\mathbf{K}_n + \eta\mathbf{I}_n))$$

where \mathbf{y}_n is the response vector of y_i 's, \mathbf{G} is the basis function matrix and each row is $\mathbf{g}(\mathbf{x}_i)^\top$. The matrix \mathbf{K}_n is the $n \times n$ kernel matrix with entries $K_{ij} = K(\mathbf{x}_i, \mathbf{x}_j; \boldsymbol{\omega})$, which is symmetric and positive definite. The likelihood function of $\mathbf{y}_n|\boldsymbol{\theta}$ is

$$p(\mathbf{y}_n|\boldsymbol{\theta}) \propto (\tau^2)^{-\frac{n}{2}} \det(\mathbf{K}_n + \eta\mathbf{I}_n)^{-1/2} \exp\left(-\frac{1}{2\tau^2}(\mathbf{y}_n - \mathbf{G}\boldsymbol{\beta})^\top(\mathbf{K}_n + \eta\mathbf{I}_n)^{-1}(\mathbf{y}_n - \mathbf{G}\boldsymbol{\beta})\right).$$

The joint posterior density is:

$$p(\boldsymbol{\theta}|\mathbf{y}_n) \propto p(\boldsymbol{\beta}|r_\beta)p(r_\beta)p(\boldsymbol{\omega}|r_\omega)p(r_\omega)p(\tau^2)p(\eta)p(\mathbf{y}_n|\boldsymbol{\theta}).$$

We summarize the conditional posterior distributions of all the parameters in Proposition 1. The detailed derivation can be found in the Supplement. Algorithm 1 summarizes the sampling procedure of sph-B²GPR.

Proposition 1. *Under the prior assumptions in (8), the conditional posterior distributions for $(\boldsymbol{\beta}, \boldsymbol{\omega}, \tau^2, \eta, r_\beta, r_\omega)$ are listed below.*

1. *The linear coefficients $\boldsymbol{\beta}$ has the following full conditional distribution*

$$\begin{aligned}
p(\boldsymbol{\beta}|\mathbf{y}_n, \boldsymbol{\omega}, \tau^2, \eta) &\propto \\
\exp\left(-\frac{1}{2\tau^2}\left(\boldsymbol{\beta}^\top \mathbf{G}^\top (\mathbf{K}_n + \eta\mathbf{I}_n)^{-1} \mathbf{G}\boldsymbol{\beta} - 2\boldsymbol{\beta}^\top \mathbf{G}^\top (\mathbf{K}_n + \eta\mathbf{I}_n)^{-1} \mathbf{y}_n\right)\right) &\mathbb{I}(\|\boldsymbol{\beta}\|_q \leq r_\beta).
\end{aligned}$$

Therefore, $\boldsymbol{\beta}$ follows a truncated multivariate normal distribution specified below

$$\boldsymbol{\beta}|\mathbf{y}_n, \boldsymbol{\omega}, \tau^2, \eta \sim \mathcal{MVN}_p(\hat{\boldsymbol{\beta}}_n, \boldsymbol{\Sigma}_{\boldsymbol{\beta}|n})$$

with

$$\boldsymbol{\Sigma}_{\boldsymbol{\beta}|n} = \left[\frac{1}{\tau^2} \mathbf{G}^\top (\mathbf{K}_n + \eta\mathbf{I}_n)^{-1} \mathbf{G}\right]^{-1}, \quad \hat{\boldsymbol{\beta}}_n = \boldsymbol{\Sigma}_{\boldsymbol{\beta}|n} \frac{\mathbf{G}^\top (\mathbf{K}_n + \eta\mathbf{I}_n)^{-1} \mathbf{y}_n}{\tau^2}.$$

2. *The radius parameter r_β for $\boldsymbol{\beta}$ has the following full conditional distribution*

$$\begin{aligned}
p(r_\beta|\mathbf{y}_n, \boldsymbol{\theta}_\beta, \boldsymbol{\omega}, \tau^2, \eta) &\propto \\
\exp\left(-\frac{1}{2\tau^2}(\mathbf{y}_n - \mathbf{G}(sgn(\boldsymbol{\theta}_\beta) \circ |\boldsymbol{\theta}_\beta|^{\frac{2}{q}} r_\beta))^\top (\mathbf{K}_n + \eta\mathbf{I}_n)^{-1} (\mathbf{y}_n - \mathbf{G}(sgn(\boldsymbol{\theta}_\beta) \circ |\boldsymbol{\theta}_\beta|^{\frac{2}{q}} r_\beta))\right)
\end{aligned}$$

where $\boldsymbol{\theta}_\beta = (\theta_{\beta_1}, \dots, \theta_{\beta_p})^\top$ with θ_{β_i} defined at the end of Section 4.2 and “ \circ ” is the Hadamard product (element-wise product).

3. The correlation parameters $\boldsymbol{\omega}$ have the following full conditional distribution

$$p(\boldsymbol{\omega} | \mathbf{y}_n, \boldsymbol{\beta}, \tau^2, \eta) \propto \det(\mathbf{K}_n + \eta \mathbf{I}_n)^{-\frac{1}{2}} \\ \times \exp \left(-\frac{1}{2\tau^2} (\mathbf{y}_n - \mathbf{G}\boldsymbol{\beta})^\top (\mathbf{K}_n + \eta \mathbf{I}_n)^{-1} (\mathbf{y}_n - \mathbf{G}\boldsymbol{\beta}) \right) \mathbb{I}(\|\boldsymbol{\omega}\|_q \leq r_\omega)$$

where the kernel matrix \mathbf{K}_n has entries $K_{ij} = K(\mathbf{x}_i, \mathbf{x}_j, \boldsymbol{\omega})$.

4. The radius parameter r_ω for $\boldsymbol{\omega}$ has the following full conditional distribution

$$p(r_\omega | \mathbf{y}_n, \boldsymbol{\beta}, \boldsymbol{\theta}_\omega, \tau^2, \eta) \propto \det(\mathbf{K}_n + \eta \mathbf{I}_n)^{-\frac{1}{2}} \\ \times \exp \left(-\frac{1}{2\tau^2} (\mathbf{y}_n - \mathbf{G}\boldsymbol{\beta})^\top (\mathbf{K}_n + \eta \mathbf{I}_n)^{-1} (\mathbf{y}_n - \mathbf{G}\boldsymbol{\beta}) \right).$$

The kernel matrix \mathbf{K}_n depends on r_ω and $\boldsymbol{\theta}_\omega$

$$K_{ij} = K(\mathbf{x}_i, \mathbf{x}_j; \boldsymbol{\omega}) = \exp \left\{ -r_\omega^2 \sum_{k=1}^d |\theta_{\omega_k}|^{\frac{4}{q}} (x_{ik} - x_{jk})^2 \right\}.$$

where $\boldsymbol{\theta}_\omega = (\theta_{\omega_1}, \dots, \theta_{\omega_d})^\top$ with θ_{ω_i} defined at the end of Section 4.2.

5. The variance parameter τ^2 has the following full conditional distribution

$$\tau^2 | \mathbf{y}_n, \boldsymbol{\beta}, \boldsymbol{\omega}, \eta \sim \text{Scaled Inverse-}\chi^2(df_{\tau^2} + n, \hat{\tau}^2),$$

with

$$\hat{\tau}^2 = \frac{1 + (\mathbf{y}_n - \mathbf{G}\boldsymbol{\beta})^\top (\mathbf{K}_n + \eta \mathbf{I}_n)^{-1} (\mathbf{y}_n - \mathbf{G}\boldsymbol{\beta})}{df_{\tau^2} + n}.$$

6. The nugget parameter η has the following full conditional distribution

$$p(\eta | \mathbf{y}_n, \boldsymbol{\beta}, \boldsymbol{\omega}, \tau^2) \propto \eta^{a_\eta - 1} e^{-b_\eta \eta} \det(\mathbf{K}_n + \eta \mathbf{I}_n)^{-\frac{1}{2}} \\ \times \exp \left(-\frac{1}{2\tau^2} (\mathbf{y}_n - \mathbf{G}\boldsymbol{\beta})^\top (\mathbf{K}_n + \eta \mathbf{I}_n)^{-1} (\mathbf{y}_n - \mathbf{G}\boldsymbol{\beta}) \right).$$

4.3 Sampling for hmc-B²GPR

For the hmc-B²GPR method, we use the informative prior distributions on all the parameters $\boldsymbol{\theta} = (\boldsymbol{\beta}, \nu_\beta^2, \boldsymbol{\omega}, \nu_\omega^2, \tau^2, \eta)$, which are specified as follows.

$$\begin{aligned} \boldsymbol{\beta} | \nu_\beta^2 &\sim \mathcal{MVN}_p(\mathbf{0}, \nu_\beta^2 \mathbf{R}), \quad \nu_\beta^2 \sim \text{Inverse-}\Gamma(a_\beta, b_\beta) \\ \omega_i | \nu_\omega^2 &\stackrel{\text{i.i.d.}}{\sim} \mathcal{N}(0, \nu_\omega^2), \text{ for } i = 1, \dots, d, \quad \nu_\omega^2 \sim \text{Inverse-}\Gamma(a_\omega, b_\omega) \\ \tau^2 &\sim \text{Inverse-}\chi^2(df_{\tau^2}), \quad \eta \sim \Gamma(a_\eta, b_\eta). \end{aligned} \tag{9}$$

The correlation matrix \mathbf{R} is taken to be diagonal, $\mathbf{R} = \text{diag}\{1, \rho, \dots, \rho, \rho^2, \dots, \rho^2, \dots\}$. Here we let $\rho = 0.5$. The power of ρ is the same as the order of the corresponding polynomial

Algorithm 1 Sampling procedure for sph-B²GPR.

- 1: Set the hyperparameters $a_\eta, b_\eta, df_{\tau^2}$, the number of samples in the burn-in period (denoted by B), and the total number of samples of the MCMC chain (denoted by T).
- 2: Initialize $\beta^{(0)}, r_\beta^{(0)}, \omega^{(0)}, r_\omega^{(0)}, \tau^{2(0)}, \eta^{(0)}$.
- 3: **for** $t = 1$ to T **do**
- 4: Sample $\beta^{(t)}$ from $p(\beta | \mathbf{y}_n, \omega^{(t-1)}, \tau^{2(t-1)}, \eta^{(t-1)})$ through Algorithm S2 with constraint $\|\beta^{(t)}\|_q \leq r_\beta^{(t-1)}$.
- 5: Sample $r_\beta^{(t)}$ from $p(r_\beta | \mathbf{y}_n, \theta_\beta^{(t)}, \omega^{(t-1)}, \tau^{2(t-1)}, \eta^{(t-1)})$ through Metropolis-Hastings (MH) method.
- 6: Sample $\omega^{(t)}$ from $p(\omega | \mathbf{y}_n, \beta^{(t)}, \tau^{2(t-1)}, \eta^{(t-1)})$ through Algorithm S2 with constraint $\|\omega^{(t)}\|_q \leq r_\omega^{(t-1)}$.
- 7: Sample $r_\omega^{(t)}$ from $p(r_\omega | \mathbf{y}_n, \beta^{(t)}, \theta_\omega^{(t)}, \tau^{2(t-1)}, \eta^{(t-1)})$ through MH.
- 8: Sample $\tau^{2(t)}$ from $p(\tau^2 | \mathbf{y}_n, \beta^{(t)}, \omega^{(t)}, \eta^{(t-1)})$ through Inverse- χ^2 posterior distribution.
- 9: Sample $\eta^{(t)}$ from $p(\eta | \mathbf{y}_n, \beta^{(t)}, \omega^{(t)}, \tau^{2(t)}, \eta^{(t-1)})$ through MH.
- 10: **end for**
- 11: Remove the initial B samples from the burn-in period. Use the remaining samples to perform prediction and inference tasks.

term. For example, for the model $\mathbf{g}(\mathbf{x}) = [1, x_1, x_2, x_1^2, x_1 x_2, x_2^2]$, the correlation matrix should be $\mathbf{R} = \text{diag}\{1, \rho, \rho, \rho^2, \rho^2, \rho^2\}$. In this way the prior variance decrease exponentially as the order of the polynomial terms, following the hierarchy ordering principle (Wu and Hamada, 2011), which reduces the size of the model and avoid including higher order and less significant model terms. Such prior distribution was firstly proposed by Joseph (2006), and later used by Kang and Joseph (2009); Ai et al. (2009); Kang et al. (2018).

The sampling distribution of $\mathbf{y}_n | \boldsymbol{\theta}$ is the same as in sph-B²GPR and the joint posterior density is

$$\begin{aligned} p(\boldsymbol{\theta} | \mathbf{y}_n) &\propto p(\boldsymbol{\theta}) p(\mathbf{y}_n | \boldsymbol{\theta}) \\ &\propto p(\beta | \nu_\beta^2) p(\nu_\beta^2) p(\omega | \nu_\omega^2) p(\nu_\omega^2) p(\tau^2) p(\eta) p(\mathbf{y}_n | \boldsymbol{\theta}). \end{aligned}$$

Due to conditional conjugacy, some posterior distributions are directly available, as summarized in the following proposition.

Proposition 2. *Under the prior distributions in (9), the conditional posterior distributions for all the parameters are derived as follows.*

1. *The full conditional distribution for β is*

$$\beta | \mathbf{y}_n, \nu_\beta^2, \omega, \tau^2, \eta \sim \mathcal{MVN}_p(\hat{\beta}_n, \Sigma_{\beta|n}),$$

where

$$\Sigma_{\beta|n} = \left[\frac{1}{\tau^2} \mathbf{G}^\top (\mathbf{K}_n + \eta \mathbf{I}_n)^{-1} \mathbf{G} + \frac{1}{\nu_\beta^2} \mathbf{R}^{-1} \right]^{-1}, \quad \hat{\beta}_n = \Sigma_{\beta|n} \frac{\mathbf{G}^\top (\mathbf{K}_n + \eta \mathbf{I}_n)^{-1} \mathbf{y}_n}{\tau^2}.$$

2. The full conditional distribution for ν_β^2 is

$$\nu_\beta^2 | \boldsymbol{\beta}, \boldsymbol{\omega}, \tau^2, \eta, \mathbf{y}_n \sim \text{Inverse-}\Gamma \left(a_\beta + \frac{p}{2}, \frac{1}{2} \boldsymbol{\beta}^\top \mathbf{R}^{-1} \boldsymbol{\beta} + b_\beta \right).$$

3. The full conditional distribution for the correlation parameters $\boldsymbol{\omega}$ is

$$\begin{aligned} p(\boldsymbol{\omega} | \boldsymbol{\beta}, \nu_\omega^2, \tau^2, \eta, \mathbf{y}_n) &\propto \det(\mathbf{K}_n + \eta \mathbf{I}_n)^{-\frac{1}{2}} \\ &\times \exp \left(-\frac{1}{2\tau^2} (\mathbf{y}_n - \mathbf{G}\boldsymbol{\beta})^\top (\mathbf{K}_n + \eta \mathbf{I}_n)^{-1} (\mathbf{y}_n - \mathbf{G}\boldsymbol{\beta}) - \frac{\boldsymbol{\omega}^\top \boldsymbol{\omega}}{2\nu_\omega^2} \right). \end{aligned}$$

4. The full conditional distribution for ν_ω^2 is

$$\nu_\omega^2 | \boldsymbol{\beta}, \boldsymbol{\omega}, \tau^2, \eta, \mathbf{y}_n \sim \text{Inverse-}\Gamma \left(a_\omega + \frac{d}{2}, \frac{1}{2} \sum_{i=1}^d \omega_i^2 + b_\omega \right).$$

5. The full conditional distribution for the variance parameter τ^2 and η are the same as in Proposition 1.

Unlike sph-B²GPR, which explicitly imposes hard ℓ_q -norm constraints on parameters to directly achieve sparsity via regularization, the hmc-B²GPR method uses hierarchical shrinkage priors to implicitly push sparsity through posterior concentration. Consequently, the standard HMC method relies solely on the data-driven shrinkage induced by the priors to identify and suppress irrelevant parameters. The complete MCMC sampling algorithm for hmc-B²GPR is summarized in Algorithm 2.

5 Simulation Examples

In this section, we evaluate the performance of the proposed sph- and hmc-B²GPR methods through a series of simulation studies and compare them against three alternative GP regression approaches implemented via different R packages.

- Maximum likelihood estimation (MLE)-based Gaussian Process regression.

Algorithm 2 Sampling procedure for hmc-B²GPR.

- 1: Set the hyperparameters $a_\eta, b_\eta, df_{\tau^2}, a_\beta, b_\beta, a_\omega, b_\omega$, the number of samples in the burn-in period (denoted by B), and the total number of samples of the MCMC chain (denoted by T).
- 2: Initialize $\beta^{(0)}, \nu_\beta^{2(0)}, \omega^{(0)}, \nu_\omega^{2(0)}, \tau^{2(0)}, \eta^{(0)}$
- 3: **for** $t = 1$ to T **do**
- 4: Sample $\beta^{(t)}$ from $p(\beta | \mathbf{y}_n, \nu_\beta^{2(t-1)}, \omega^{(t-1)}, \tau^{2(t-1)}, \eta^{(t-1)})$ using multivariate normal distribution.
- 5: Sample $\nu_\beta^{2(t)}$ from $p(\nu_\beta^{2(t)} | \mathbf{y}_n, \beta^{(t)}, \omega^{(t-1)}, \tau^{2(t-1)}, \eta^{(t-1)})$ through the inverse- Γ distribution.
- 6: Sample $\omega^{(t)}$ from $p(\omega | \mathbf{y}_n, \nu_\omega^{2(t-1)}, \beta^{(t)}, \tau^{2(t-1)}, \eta^{(t-1)})$ through Algorithm S1.
- 7: Sample $\nu_\omega^{2(t)}$ from $p(\nu_\omega^{2(t)} | \mathbf{y}_n, \beta^{(t)}, \omega^{(t)}, \tau^{2(t-1)}, \eta^{(t-1)})$ through inverse- Γ distribution.
- 8: Sample $\tau^{2(t)}$ from $p(\tau^{2(t)} | \mathbf{y}_n, \beta^{(t)}, \omega^{(t)}, \eta^{(t-1)})$ through inverse- χ^2 distribution.
- 9: Sample $\eta^{(t)}$ from $p(\eta^{(t)} | \mathbf{y}_n, \beta^{(t)}, \omega^{(t)}, \tau^{2(t)}, \eta^{(t-1)})$ through MH method.
- 10: **end for**
- 11: Remove the initial B samples from the burn-in period. Use the remaining samples to perform prediction and inference tasks.

- Traditional kriging method with constant, linear, and quadratic mean functions ([Santner et al., 2003](#)).
- Local approximate Gaussian Process (laGP) method by [Gramacy and Apley \(2015\)](#).

Each of these methods has distinct characteristics and is suitable for different scenarios. Specifically, MLE-based GP and kriging methods are popular approaches widely employed in surrogate modeling. The two are essentially the same except that they are implemented in different packages. In MLE-based GP, the mean is a linear function of the input. In the kriging methods, we use three mean functions of the input: constant, linear, and quadratic functions. These methods perform well when n is not large and d is small. However, their predictive accuracy may degrade for increasing d due to the absence of built-in sparsity mechanisms. The laGP, on the other hand, is tailored for larger data sets. It partitions data and fits a local GP model around each prediction point, offering computational efficiency and scalability. While laGP often provides accurate predictions with larger n , it may not adequately capture global trends or complex interactions as effectively as the full GP model. All numerical experiments in this study were performed in R ([R Core Team, 2025](#)). Specifically, the MLE-based GP, kriging, and local GP approaches were implemented using the R packages `mlegp` ([Dancik and Dorman, 2008](#)), `DiceKriging` ([Roustant et al., 2012](#)), and `laGP` ([Gramacy, 2016](#)), respectively. Table 1 summarizes the abbreviated names of

the methods employed throughout this study, along with corresponding descriptions for reference in subsequent discussions.

Table 1: Abbreviated names of the methods

Abbreviation	Full Description
mlegp	Maximum likelihood estimated GP with linear mean
laGP	Local approximate GP
krig-const	Kriging with constant mean
krig-linear	Kriging with linear mean
krig-quad	Kriging with quadratic mean
hmc-B²GPR	B ² GPR using HMC with normal shrinkage priors
sph-B²GPR-q	B ² GPR using the SphHMC with ℓ_q -norm constraint ($0 < q < 2$)

Algorithm Settings We summarize the algorithmic settings for all methods. For the sph-B²GPR method described in Algorithm 1, we set the hyperparameters in the prior distributions as follows: $a_\eta = 0.5, b_\eta = 0.5, df_{\tau^2} = 4$. For the hmc-B²GPR approach with shrinkage priors described in Algorithm 2, we use the following hyperparameters in prior distributions: $a_\eta = 0.5, b_\eta = 0.5, df_{\tau^2} = 4, a_\beta = 1, b_\beta = 1, a_\omega = 1, b_\omega = 1$. For both the HMC and the Spherical HMC (Algorithm S1 and S2), we need to specify the step size ϵ and the number of leapfrog integration steps L (the for-loop part). Following the recommendations in Lan et al. (2019) and Hoffman et al. (2014), we adopt the dual averaging scheme (Nesterov, 2009) to adaptively tune the step size ϵ during the burn-in phase. We employ the “No-U-Turn” criterion as the stopping rule for the leapfrog integration, terminating when the trajectory exits the initial state, which is defined by the condition $\langle \tilde{\theta}^{(0)}, \tilde{\theta}^{(l)} \rangle < 0$. Additionally, we set the maximum leapfrog integration step number L_{max} randomly from a uniform integer distribution between 1 and 10. The initial step size is heuristically chosen following the approach in Hoffman et al. (2014).

For both Algorithm 1 and 2, we run two parallel chains. For each chain, we set the first $B = 1,600$ samples as burn-in. The total length of the chain (including burn-in) ranges from $T = 3,000$ to $T = 6,000$. The actual chain length may differ across runs because we employ a simple convergence diagnostic, i.e., if the two chains become sufficiently close at some point, the simulation is stopped early.

Performance Metrics We evaluate the performance of different methods using the standardized root-mean-square error (standardized RMSE) on the test data sets, defined as the RMSE normalized by the standard deviation of the true outputs:

$$\text{Standardized root-mean-square error} = \frac{\sqrt{\frac{1}{n} \sum_{i=1}^n (y_i - \hat{y}_i)^2}}{\sqrt{\frac{1}{n} \sum_{i=1}^n (y_i - \bar{y})^2}}$$

where y_i denotes the true output, \hat{y}_i is the predicted output from the model, and \bar{y} is the mean of the true outputs. Additionally, we illustrate the box plots of the point estimates (sample medians) of the parameters β and correlation parameters ω from all repeated simulations. Note that they are not the posterior samples from one simulation, but just the point estimates, which is why all the box plots show little variation. In each simulation, we check whether the 95% credible intervals (obtained from sample quantiles) of the parameters β and ω include zero. If zero is included in the confidence intervals, it means that the corresponding β_i or ω_i are not statistical significant, otherwise significant. The color shade of the box plots indicates the frequencies when β_i or ω_i are identified to be significant. The darker the color is, the more significant the corresponding parameter is.

5.1 Pre-specified Gaussian Process

In this example, we simulate data from a pre-specified Gaussian process model (1) in Section 2 with input dimension $d = 5$. The true parameters of the GP are set as follows: the intercept $\beta_0 = 3$, the coefficient of the linear terms $\beta = (-2, 2, -4, 4, 3)$, the correlation parameters $\omega = (1, 1.5, 2, 2.5, 3)$, and the variance parameter $\tau^2 = 1$. For each simulation, we generate $n = 200$ training data. The input data \mathbf{x}_i 's are from a 5-dimensional maximin Latin hypercube design (Carnell, 2024) within the domain $[0, 1]^5$ and the output $y(\mathbf{x}_i)$ is simulated from the GP without noise ϵ . An additional design of 1000 input points is generated using a random Latin hypercube design within the same domain, and the responses are simulated from the GP based on these inputs to form the test data set for evaluating prediction accuracy. Table 2 shows the average of the standardized RMSE over 100 simulations. Figure 1 shows the box plots of the point estimates of the parameters for β and ω from the method sph-B²GPR with $q = 1.8$. The dark shade of the box plots indicates that all β and ω are significant. Figure 2 and 3 present the posterior histograms

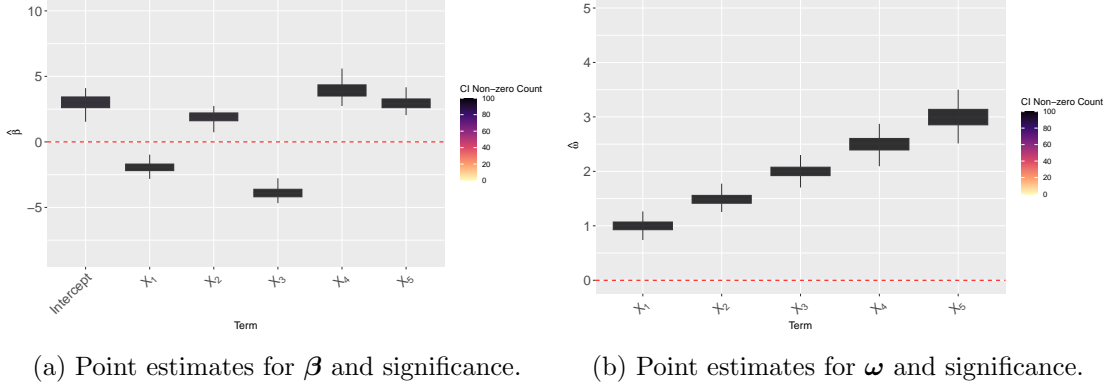


Figure 1: Box plots of the point estimates of the parameters for the pre-specified GP.

for each β and ω in one simulation produced by sph-B²GPR with $q = 1.8$. The red vertical lines are the true parameter values of the underlying GP model.

Table 2: Standardized RMSE (100 replicates for $n = 200$) for pre-specified Gaussian Process

	mlegp	laGP	krig-const	krig-linear	hmc-B ² GPR	sph-B ² GPR-0.8	sph-B ² GPR-1	sph-B ² GPR-1.8
Mean	0.0260	0.1091	0.0799	0.0270	0.0303	0.0267	0.0264	0.0260
SD	0.0082	0.0427	0.0139	0.0087	0.0139	0.0086	0.0082	0.0083

Performance Summary The method sph-B²GPR with $q = 1.8$ and mlegp both have the best performance in terms of average standardized RMSE ($\approx 2.6 \times 10^{-2}$) and stability (small standard deviation). As q becomes smaller, sph-B²GPR performs slightly worse. But compared to sph-B²GPR, hmc-B²GPR is only better than laGP and krig-const. For the parameter β and ω , the posterior medians closely match the true values, and the 95% confidence intervals rarely include zero, correctly flagging all as significant. Each posterior histogram for β and ω is unimodal and centered around the true parameter values. This aligns with the low standardized RMSE observed, indicating accurate parameter estimation by the proposed method.

5.2 Benchmark functions: Borehole, OTL Circuit, and Piston

In this example, we use three benchmark test functions from literature: the Borehole function to model water flow through a borehole, the OTL Circuit function to simulate the behavior of an electronic circuit, and the Piston function to model the circular motion of

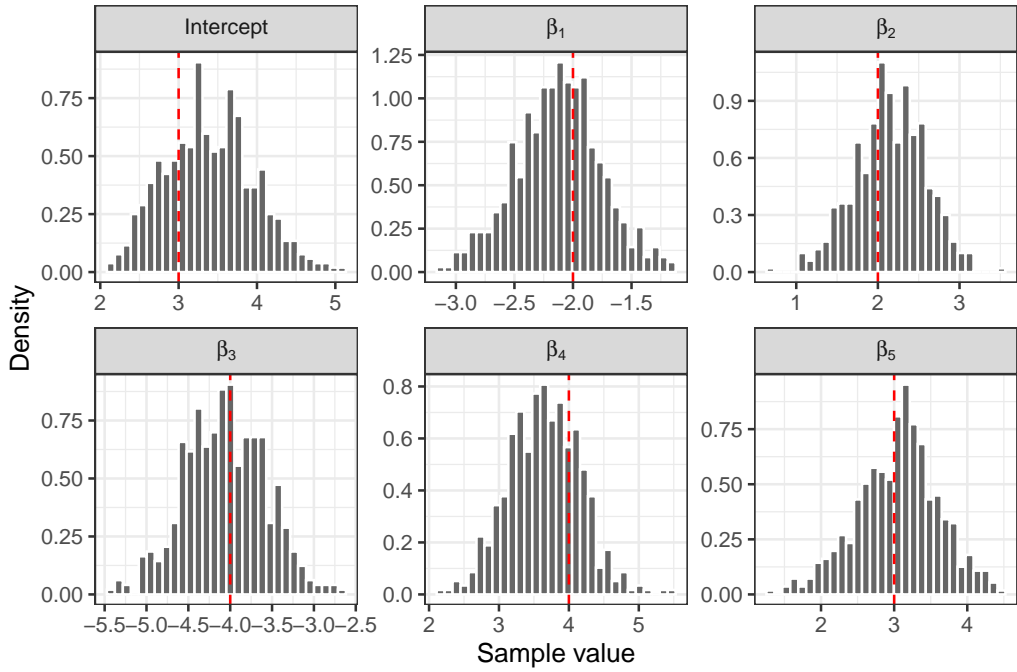


Figure 2: Posterior histograms for β in one simulation by sph-B²GPR with $q = 1.8$ for the pre-specified GP.

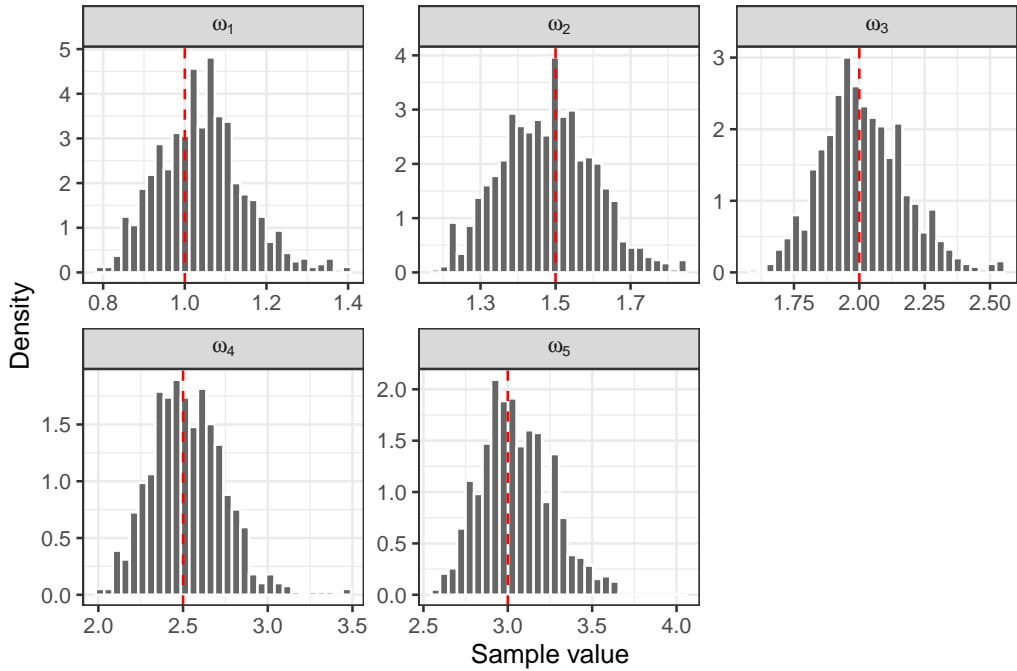


Figure 3: Posterior histograms for ω in one simulation by sph-B²GPR with $q = 1.8$ for the pre-specified GP.

a piston within a cylinder (Surjanovic and Bingham, n.d.). Their definitions are given in the Supplement. Due to limited space, we moved all the figures for this subsection to the Supplement.

For each benchmark, we generate training data sets of size $n \in \{200, 500\}$ with input from a maximin Latin hypercube design (Carnell, 2024) in $[0, 1]^d$. Then we scale the inputs to their respective physical ranges defined by the test functions. Outputs are generated from the benchmark functions with added small noise. A separate test data set of size 1000 with inputs generated from a random Latin hypercube design and outputs generated from the benchmark functions with added noise of the same distribution as the training data. We report the mean and standard deviation of the standardized RMSE over 100 simulations for each benchmark in Table 3. Figures S1– S6 show the box plots of the point estimates for the parameters β and ω with $q = 0.8$ for each benchmark function with $n = 200$ and $n = 500$. The mean functions of the GP for both sph- and hmc-B²GPR are quadratic polynomials including intercept, linear, quadratic, and interaction terms.

We then augment the input with additional irrelevant input variables to test the variable selection capability of the proposed B²GPR methods in a high-dimensional setting. Specifically, we increase the input dimension to $d = 20$ for each of the three functions. Only the original input variables should be significant. The training and testing data sets are generated in the same way as earlier. Table 4 summarizes the average performance measures of the methods over 100 replicates for all three functions with high-dimensional inputs, including the mean and standard deviation of the standardized RMSE. Figures S7– S12 show the box plots of the point estimates for the parameters β and ω with $q = 0.8$ for all test functions of $n = 200$ and 500. The mean functions of the GP for both sph- and hmc-B²GPR are linear polynomials for $d = 20$.

Borehole Function Considering the original input dimension $d = 8$, for $n = 200$, sph-B²GPR with $q = 0.8$ attains the best average standardized RMSE (0.0182) and the smallest SD (0.0019), and $q = 1$ and 1.8 fall close behind; all three sph-B²GPR variants outperform kriging, mlegp, laGP, and hmc-B²GPR. As n increases to 500, all methods improve, but sph-B²GPR remains both the most accurate and the most stable. The point estimates from Figures S1 and S2 indicate that most low- and high-order fixed-effect coefficients of β are shrunk to zero. In contrast, the correlation parameters ω are clearly significant for five

input variables (r_w , H_u , H_l , L , and K_w) for both $n = 200$ and 500 . These identified active input variables agree with the discussion in [Harper et al. \(1983\)](#), confirming the B²GPR method is capable of correctly identifying relevant inputs. For the case with increased input dimension $d = 20$, sph-B²GPR is remarkably robust. The standardized RMSEs and the standard deviations remain small, whereas hmc-B²GPR exhibits much larger variability, and kriging/mlegp degrade notably. The laGP is especially sensitive to the increased dimensions for $n = 200$. The box plots in Figures [S7](#) and [S8](#) are consistent with the $d = 8$ cases on the significant ω 's.

OTL Circuit Function For $d = 6$ and $n = 200$, sph-B²GPR with $q = 0.8$ attains the best average standardized RMSE (0.0188) and the smallest SD (0.0019), with $q = 1$ and 1.8 are slightly worse. The hmc-B²GPR has a similar mean standardized RMSE with sph-B²GPR-1.8. As n increases to 500, sph-B²GPR remains both the most accurate and the most stable. For the lower-order fixed-effect coefficients β , the identified significant terms are X_3 and X_4 , X_1 , and X_2 show weaker linear effects for $n = 200$, while other terms are nearly zero. As n increases to 500, X_1 and X_2 show slightly stronger linear effects. For the 2nd order β , X_3X_4 and X_4^2 show notable significance, while others are negligible. For correlation parameters ω , the identified significant inputs are X_1 and X_2 for both sample sizes. Overall, the sph-B²GPR method effectively identifies active inputs for X_1 , X_2 , X_3 , and X_4 , which agrees with the paper [Moon \(2010\)](#). For the case with increased input dimension $d = 20$, sph-B²GPR is still the winner, whereas hmc-B²GPR remains competitive but exhibits much larger variability. Among the $d = 20$ dimensions, sph-B²GPR only identifies the first four correlation parameters $\omega_1, \dots, \omega_4$ as significant, which is consistent with the $d = 6$ and $n = 500$ case.

Piston Function For the original input dimension $d = 7$, when $n = 200$ or 500, sph-B²GPR achieves the smallest average standardized RMSEs and the smallest variation under different q values. None of the fixed effects β is significant. For the correlation parameters ω , the input variables X_1 , X_2 , X_3 , and X_4 are significant, and X_5 shows weak significance, while coefficients for X_6 and X_7 are nearly zero, which agrees with the findings in [\(Moon, 2010\)](#). For the case with increased input dimension $d = 20$, sph-B²GPR still outperforms the others and identifies the same significant input variables as in the $d = 7$ case.

To sum up the three examples, the sph-B²GPR with different q values has consistently

outperformed the other methods, in terms of prediction accuracy and variable selection for both the mean and correlation functions of the GP. Although worse than sph-B²GPR, the hmc-B²GPR has similar performance compared to the best of the alternative methods.

Table 3: Standardized RMSE for the three benchmark test functions: Borehole, OTL Circuit, Piston.

Function	Size	mlegp	laGP	krig-const	krig-linear	krig-quad	hmc-B ² GPR	sph-B ² GPR-0.8	sph-B ² GPR-1	sph-B ² GPR-1.8
Borehole (8-dim)	$n = 200$	0.0608 (0.0043)	0.0389 (0.0029)	0.0342 (0.0027)	0.0306 (0.0024)	0.0355 (0.0069)	0.0398 (0.0077)	0.0182 (0.0019)	0.0187 (0.0024)	0.0207 (0.0034)
	$n = 500$	0.0539 (0.0026)	0.0212 (0.0013)	0.0216 (0.0014)	0.0196 (0.0013)	0.0171 (0.0014)	0.0151 (0.0036)	0.0121 (0.0011)	0.0124 (0.0011)	0.0125 (0.0015)
OTL Circuit (6-dim)	$n = 200$	0.0539 (0.0040)	0.0284 (0.0034)	0.0272 (0.0019)	0.0250 (0.0019)	0.0271 (0.0045)	0.0216 (0.0032)	0.0188 (0.0019)	0.0209 (0.0060)	0.0198 (0.0038)
	$n = 500$	0.0484 (0.0026)	0.0172 (0.0011)	0.0173 (0.0012)	0.0164 (0.0012)	0.0193 (0.0034)	0.0143 (0.0018)	0.0142 (0.0016)	0.0141 (0.0019)	0.0138 (0.0025)
Piston (7-dim)	$n = 200$	0.0749 (0.0075)	0.0721 (0.0111)	0.0637 (0.0052)	0.0585 (0.0051)	0.0645 (0.0262)	0.0522 (0.0248)	0.0438 (0.0047)	0.0436 (0.0049)	0.0435 (0.0046)
	$n = 500$	0.0597 (0.0042)	0.0422 (0.0081)	0.0383 (0.0029)	0.0360 (0.0030)	0.0337 (0.0026)	0.0313 (0.0210)	0.0272 (0.0024)	0.0272 (0.0023)	0.0271 (0.0024)

Note: Each cell reports the mean (first line) and standard deviation (second line, in parentheses) of standardized RMSE across 100 replicates; lower is better. Bold indicates the best (lowest) mean in each row. All ties are in bold.

6 Case Study: H₂O Potential Energy

We demonstrate the proposed B²GPR method on a real molecular data set. Following the “H₂O Potential Energy: A Hands-On Example” in [Deringer et al. \(2021\)](#), we consider the problem of learning the potential energy surface for a water molecule using Gaussian process regression. The dataset comprises 121 configurations arranged on an 11×11 grid, uniquely determined by two O-H bond lengths and the H-O-H angle.

Following the preprocessing pipeline in [Deringer et al. \(2021\)](#), we construct descriptors using the Smooth Overlap of Atomic Positions (SOAP) method, incorporating O-H bond lengths, H-O-H angle, molecular dipole vector, and the so-called atomic lines (element, position, and force for each atom). The SOAP hyperparameters are set as in [Deringer et al. \(2021\)](#). This results in an initial feature matrix with 952 channels per configuration. Because this is a small three-atom system sampled on a structured grid, several SOAP channels are identical across configurations; we remove zero-variance columns, leaving 316 features.

Table 4: Standardized RMSE with increased input dimensions $d = 20$ for the benchmark test functions.

Function	Size	mlegp	laGP	krig-const	krig-linear	hmc- B^2GPR	sph- $B^2GPR-0.8$	sph- B^2GPR-1	sph- $B^2GPR-1.8$
Borehole (20-dim)	$n = 200$	0.0629 (0.0107)	0.3869 (0.6684)	0.0994 (0.0086)	0.0577 (0.0045)	0.0665 (0.0855)	0.0179 (0.0018)	0.0181 (0.0019)	0.0185 (0.0021)
	$n = 500$	0.0540 (0.0153)	0.0666 (0.0037)	0.0664 (0.0037)	0.0385 (0.0024)	0.0520 (0.0823)	0.0121 (0.0010)	0.0122 (0.0010)	0.0123 (0.0010)
OTL (20-dim)	$n = 200$	0.0631 (0.0116)	0.1571 (0.0122)	0.1094 (0.0069)	0.0494 (0.0033)	0.0635 (0.0615)	0.0189 (0.0015)	0.0190 (0.0015)	0.0201 (0.0041)
	$n = 500$	0.0481 (0.0082)	0.0866 (0.0065)	0.0722 (0.0036)	0.0334 (0.0018)	0.0358 (0.0512)	0.0121 (0.0011)	0.0122 (0.0011)	0.0126 (0.0011)
Piston (20-dim)	$n = 200$	0.0827 (0.0188)	0.2179 (0.0316)	0.1369 (0.0109)	0.0949 (0.0089)	0.1395 (0.1251)	0.0438 (0.0041)	0.0445 (0.0067)	0.0451 (0.0046)
	$n = 500$	0.0608 (0.0141)	0.1147 (0.0073)	0.0936 (0.0055)	0.0645 (0.0045)	0.0761 (0.1024)	0.0276 (0.0027)	0.0276 (0.0026)	0.0278 (0.0026)

Note: Each cell reports the mean (first line) and standard deviation (second line, in parentheses) of standardized RMSE across 100 replicates; lower is better. Bold indicates the best (lowest) mean in each row. All ties are in bold.

We then split the data set into a training set of size $n = 100$ and a test set of size 21. However, with 316 features and only 100 training samples, this remains a challenging problem, and directly applying any regression model is likely to lead to severe overfitting and numerical instability. To address this, we perform principal component analysis (PCA) on the feature matrix for the training set only and retain the first 50 principal components as the input variables. Test configurations are projected using the same loadings. This yields a more manageable 50-dimensional input space for regression. We evaluate out-of-sample prediction accuracy on the 21 test configurations and repeat the random train-test split 100 times to assess variability. Table 5 reports the mean and standard deviation of standardized RMSE over these 100 replicates. Across the 100 simulations, the sph- B^2GPR methods achieve the best accuracy with extremely small variation, outperforming all counterparts by wide margins. The potential energy surface for water molecules is smooth and essentially a low-dimensional function after SOAP featurization and PCA. In this setting, the spherical-constrained posterior places mass on a small region of the parameter space, guiding the sampler to explore the high-probability region effectively. This leads to accurate and stable predictions.

Table 5: Standardized RMSE (100 replicates for $n = 100$) for the water-molecule dataset

	mlegp	laGP	krig- const	hmc- B^2 GPR	sph- B^2 GPR-0.8	sph- B^2 GPR-1	sph- B^2 GPR-1.8
Mean	0.9780	0.0342	0.3537	0.1877	0.0002	0.0003	0.0002
SD	0.0508	0.0827	0.1551	0.3921	0.0003	0.0014	0.0005

7 Conclusion

In this paper, we proposed Bayesian Bridge Gaussian Process Regression (B^2 GPR), a Gaussian process regression framework that regularizes both the linear fixed-effect coefficients β and correlation parameters ω via ℓ_q -norm constraints. We suggested two different versions of B^2 GPR, depending on the regularization norm q . When $0 < q < 2$, we use non-informative bounded priors for β and ω , and the modes of the conditional posterior distributions of β and ω are equivalent to the solutions of MLE with ℓ_q -norm regularization. To sample efficiently from the resulting constrained posterior, we adopted the Spherical Hamiltonian Monte Carlo scheme that enforces the constraints exactly by mapping the parameter space to a sphere and running Hamiltonian dynamics on that manifold. This preserves the advantages of standard HMC (geometry-aware proposals and effective global moves) while providing direct control over sparsity and regularization strength. This version is named sph- B^2 GPR for short. When $q = 2$, we use the informative Gaussian priors for β and ω , and the posterior modes are equivalent to the solution of MLE with ℓ_2 -norm regularization. Regular sampling methods can be used here. We choose the standard HMC for ω and the Metropolis-Hastings sampler for other parameters if their conditional posteriors are not any known distributions.

Through the controlled simulations (a pre-specified GP), three standard benchmarks (Borehole, OTL circuit, and Piston functions), and a real molecular dataset (the water potential energy surface), the proposed B^2 GPR, particularly sph- B^2 GPR, consistently delivers (i) *high predictive accuracy*, achieving the lowest or near-lowest prediction error, often by a clear margin over competing approaches; (ii) *greater robustness*, with much smaller variability across replicates; and (iii) *enhanced interpretability*, with posterior credible intervals for β and ω that clearly recover known active inputs in the benchmark problems. These advantages are persistent in high-dimensional settings with many irrelevant inputs, where

classical methods degrade noticeably and hierarchical-prior HMC exhibits high variability. The proposed sph-B²GPR sampler therefore offers a practical way to simultaneously perform variable selection and inference in GP regression.

Supplementary materials

The supplement includes the in-depth reviews of HMC and SphHMC, definitions of the three benchmark functions, figures for the estimated parameter values for all simulation settings for the three benchmark examples, and the derivations for Proposition 1 and 2.

References

Ai, M., Kang, L., and Joseph, V. R. (2009), “Bayesian optimal blocking of factorial designs,” *Journal of Statistical Planning and Inference*, 139(9), 3319–3328.

Bishop, C. M. (2006), *Pattern recognition and machine learning*, New York: Springer.

Carnell, R. (2024), *lhs: Latin Hypercube Samples*. R package version 1.2.0.
URL: <https://CRAN.R-project.org/package=lhs>

Dancik, G. M., and Dorman, K. S. (2008), “mlegp: statistical analysis for computer models of biological systems using R,” *Bioinformatics*, 24(17), 1966–1967.

Deringer, V. L., Bartók, A. P., Bernstein, N., Wilkins, D. M., Ceriotti, M., and Csányi, G. (2021), “Gaussian process regression for materials and molecules,” *Chemical reviews*, 121(16), 10073–10141.

Frank, L. E., and Friedman, J. H. (1993), “A statistical view of some chemometrics regression tools,” *Technometrics*, 35(2), 109–135.

Gramacy, R. B. (2016), “laGP: large-scale spatial modeling via local approximate Gaussian processes in R,” *Journal of Statistical Software*, 72, 1–46.

Gramacy, R. B., and Apley, D. W. (2015), “Local Gaussian process approximation for large computer experiments,” *Journal of Computational and Graphical Statistics*, 24(2), 561–578.

Harper, W. V., Gupta, S. K. et al. (1983), *Sensitivity/uncertainty analysis of a borehole scenario comparing Latin hypercube sampling and deterministic sensitivity approaches*, Columbus, OH: Office of Nuclear Waste Isolation, Battelle Memorial Institute.

Hastie, T., Tibshirani, R., Friedman, J. H., and Friedman, J. H. (2009), *The elements of statistical learning: data mining, inference, and prediction*, Vol. 2, New York: Springer.

Hoerl, A. E., and Kennard, R. W. (1970), “Ridge regression: Biased estimation for nonorthogonal problems,” *Technometrics*, 12(1), 55–67.

Hoffman, M. D., Gelman, A. et al. (2014), “The No-U-Turn sampler: adaptively setting path lengths in Hamiltonian Monte Carlo,” *J. Mach. Learn. Res.*, 15(1), 1593–1623.

Hu, Z., and Dey, D. K. (2024), “Generalized variable selection algorithms for Gaussian process models by LASSO-Like penalty,” *Journal of Computational and Graphical Statistics*, 33(2), 477–486.

Hung, Y. (2011), “Penalized blind kriging in computer experiments,” *Statistica Sinica*, pp. 1171–1190.

Joseph, V. R. (2006), “A Bayesian approach to the design and analysis of fractionated experiments,” *Technometrics*, 48(2), 219–229.

Kang, L., and Joseph, V. R. (2009), “Bayesian optimal single arrays for robust parameter design,” *Technometrics*, 51(3), 250–261.

Kang, L., Kang, X., Deng, X., and Jin, R. (2018), “A Bayesian hierarchical model for quantitative and qualitative responses,” *Journal of Quality Technology*, 50(3), 290–308.

Lan, S., Holbrook, A., Elias, G. A., Fortin, N. J., Ombao, H., and Shahbaba, B. (2019), “Flexible Bayesian dynamic modeling of correlation and covariance matrices,” *Bayesian analysis*, 15(4), 1199.

Lan, S., and Kang, L. (2023), “Sampling constrained continuous probability distributions: A review,” *Wiley Interdisciplinary Reviews: Computational Statistics*, 15(6), e1608.

Lan, S., and Shahbaba, B. (2016), “Algorithmic Advances in Riemannian Geometry and Applications,”.

Lan, S., Zhou, B., and Shahbaba, B. (2014), Spherical Hamiltonian Monte Carlo for constrained target distributions,, in *International Conference on Machine Learning*, PMLR, pp. 629–637.

Li, R., and Sudjianto, A. (2005), “Analysis of computer experiments using penalized likelihood in Gaussian Kriging models,” *Technometrics*, 47(2), 111–120.

Mallick, H., and Yi, N. (2018), “Bayesian bridge regression,” *Journal of applied statistics*, 45(6), 988–1008.

Moon, H. (2010), Design and analysis of computer experiments for screening input variables, PhD thesis, The Ohio State University.

Neal, R. (2011), “MCMC Using Hamiltonian Dynamics,” *Handbook of Markov Chain Monte Carlo*, pp. 113–162.

Nesterov, Y. (2009), “Primal-dual subgradient methods for convex problems,” *Mathematical programming*, 120(1), 221–259.

Park, T., and Casella, G. (2008), “The bayesian lasso,” *Journal of the American Statistical Association*, 103(482), 681–686.

Peng, C.-Y., and Wu, C. J. (2014), “On the choice of nugget in kriging modeling for deterministic computer experiments,” *Journal of Computational and Graphical Statistics*, 23(1), 151–168.

Polson, N. G., Scott, J. G., and Windle, J. (2014), “The bayesian bridge,” *Journal of the Royal Statistical Society: Series B (Statistical Methodology)*, 76(4), 713–733.

R Core Team (2025), *R: A Language and Environment for Statistical Computing*, R Foundation for Statistical Computing, Vienna, Austria.

URL: <https://www.R-project.org/>

Roustant, O., Ginsbourger, D., and Deville, Y. (2012), “DiceKriging, DiceOptim: Two R packages for the analysis of computer experiments by kriging-based metamodeling and optimization,” *Journal of statistical software*, 51, 1–55.

Santner, T. J., Williams, B. J., Notz, W. I., and Williams, B. J. (2003), *The design and analysis of computer experiments*, Vol. 1, New York: Springer.

Surjanovic, S., and Bingham, D. (n.d.), “Virtual Library of Simulation Experiments: Test Functions and Datasets,” Retrieved December 14, 2022, from <http://www.sfu.ca/~ssurjano>.

Tibshirani, R. (1996), “Regression shrinkage and selection via the lasso,” *Journal of the Royal Statistical Society Series B: Statistical Methodology*, 58(1), 267–288.

Williams, C. K., and Rasmussen, C. E. (2006), *Gaussian processes for machine learning*, Cambridge, MA: The MIT press.

Wu, C. J., and Hamada, M. S. (2011), *Experiments: planning, analysis, and optimization*, Vol. 552, New Jersey: John Wiley & Sons.

Zhang, F., Chen, R.-B., Hung, Y., and Deng, X. (2023), “Indicator-based Bayesian variable selection for Gaussian process models in computer experiments,” *Computational Statistics & Data Analysis*, 185, 107757.

Zou, H., and Hastie, T. (2005), “Regularization and variable selection via the elastic net,” *Journal of the Royal Statistical Society Series B: Statistical Methodology*, 67(2), 301–320.

SUPPLEMENTARY MATERIAL

Review of Hamiltonian Monte Carlo and Spherical Hamiltonian Monte Carlo

Hamiltonian Monte Carlo (HMC) (Neal, 2011) is an MCMC method that uses Hamiltonian dynamics to efficiently sample from complex target distributions. By leveraging gradient information, HMC reduces random-walk behavior and yields lower autocorrelation than standard Metropolis-Hastings algorithms, enabling faster convergence.

In HMC, the sampling state consists of a position vector $\boldsymbol{\theta}$ (the parameters of interest) and a momentum vector $\boldsymbol{\phi}$ (auxiliary variables). The total energy of the system is given by the Hamiltonian:

$$H(\boldsymbol{\theta}, \boldsymbol{\phi}) = U(\boldsymbol{\theta}) + K(\boldsymbol{\phi}),$$

where $U(\boldsymbol{\theta}) = -\log p(\boldsymbol{\theta})$ is the potential energy (negative log-posterior) and $K(\boldsymbol{\phi}) = \frac{1}{2}\boldsymbol{\phi}^\top \mathbf{M}^{-1}\boldsymbol{\phi}$ is the kinetic energy. The momentum is typically distributed as $\boldsymbol{\phi} \sim \mathcal{N}(\mathbf{0}, \mathbf{M})$, where \mathbf{M} is a symmetric, positive-definite matrix known as the mass matrix. Often, it is chosen for simplicity as the identity matrix $\mathbf{M} = \mathbf{I}$.

The system evolves via Hamilton's equations:

$$\begin{aligned} \frac{d\boldsymbol{\theta}}{dt} &= \frac{\partial H(\boldsymbol{\theta}, \boldsymbol{\phi})}{\partial \boldsymbol{\phi}} = \nabla_{\boldsymbol{\phi}} K(\boldsymbol{\phi}) = \mathbf{M}^{-1} \boldsymbol{\phi} \\ \frac{d\boldsymbol{\phi}}{dt} &= -\frac{\partial H(\boldsymbol{\theta}, \boldsymbol{\phi})}{\partial \boldsymbol{\theta}} = -\nabla_{\boldsymbol{\theta}} U(\boldsymbol{\theta}) \end{aligned}$$

In practice, these equations are discretized using the leapfrog integrator. The resulting HMC algorithm (summarized in Algorithm S1) proposes new states by simulating Hamiltonian dynamics, which are then accepted or rejected via a Metropolis–Hastings step to correct for integration error. This approach enables efficient exploration of high-dimensional and correlated posterior distributions.

Algorithm S1 Hamiltonian Monte Carlo

- 1: Given the step size ϵ and current $\boldsymbol{\theta}_{t-1}$, initialize $\boldsymbol{\theta}^{(0)}$ as $\boldsymbol{\theta}_{t-1}$ and randomly sample $\boldsymbol{\phi}^{(0)} \sim \mathcal{N}(\mathbf{0}, \mathbf{M})$.
- 2: **for** $l = 0$ to $L - 1$ **do**
- 3: Update $\boldsymbol{\phi}$ by a half-step of ϵ : $\boldsymbol{\phi}^{(l+\frac{1}{2})} = \boldsymbol{\phi}^{(l)} - \frac{\epsilon}{2} \nabla_{\boldsymbol{\theta}} U(\boldsymbol{\theta}^{(l)})$.
- 4: Update $\boldsymbol{\theta}$ by a full-step of ϵ : $\boldsymbol{\theta}^{(l+1)} = \boldsymbol{\theta}^{(l)} + \epsilon \mathbf{M}^{-1} \boldsymbol{\phi}^{(l+\frac{1}{2})}$.
- 5: Update $\boldsymbol{\phi}$ by another half-step of ϵ : $\boldsymbol{\phi}^{(l+1)} = \boldsymbol{\phi}^{(l+\frac{1}{2})} - \frac{\epsilon}{2} \nabla_{\boldsymbol{\theta}} U(\boldsymbol{\theta}^{(l+1)})$.
- 6: **end for**
- 7: Compute the acceptance probability $\alpha = \min\left(1, \frac{p(\boldsymbol{\theta}^{(L)})N(\boldsymbol{\phi}^{(L)}|\mathbf{0}, \mathbf{M})}{p(\boldsymbol{\theta}_{t-1})N(\boldsymbol{\phi}_{t-1}|\mathbf{0}, \mathbf{M})}\right)$.
- 8: Accept the new state $\boldsymbol{\theta}_t = \boldsymbol{\theta}^{(L)}$ with probability α , otherwise $\boldsymbol{\theta}_t = \boldsymbol{\theta}_{t-1}$.

While HMC efficiently explores complex posterior distributions, it does not inherently handle the geometric constraints often present in statistical models. To address this, Lan et al. (2014) introduced the Spherical Hamiltonian Monte Carlo (SphHMC) as a general framework for sampling from probability distributions confined to domains bounded by arbitrary norm constraints.

The core idea of SphHMC is to use a *spherical augmentation* technique. We denote domain defined by the ℓ_q -norm constraint on the parameter $\boldsymbol{\beta} \in \mathbb{R}^d$ as $\mathcal{Q}^d := \{\boldsymbol{\beta} \in \mathbb{R}^d \mid \|\boldsymbol{\beta}\|_q \leq 1\}$, without loss of generality. It can be bijectively mapped to the d -dimensional unit ball, $\mathcal{B}_0^d(1) = \{\boldsymbol{\theta} \in \mathbb{R}^d \mid \|\boldsymbol{\theta}\|_2 \leq 1\}$, by either $\beta_i \mapsto \theta_i = \text{sgn}(\beta_i)|\beta_i|^{q/2}$ or $\boldsymbol{\beta} \mapsto \boldsymbol{\theta} = \boldsymbol{\beta} \frac{\|\boldsymbol{\beta}\|_\infty}{\|\boldsymbol{\beta}\|_2}$. [Lan and Shahbaba \(2016\)](#) used the spherical augmentation to further map the unit ball $\mathcal{B}_0^d(1)$ to the hyper-sphere \mathcal{S}^d by adding the auxiliary variable θ_{d+1} to $\boldsymbol{\theta}$. Define the extended parameter as $\tilde{\boldsymbol{\theta}} = (\boldsymbol{\theta}, \theta_{d+1}) \in \mathcal{S}^d$. The lower hemisphere of \mathcal{S}^d corresponds to $\theta_{d+1} = -\sqrt{1 - \|\boldsymbol{\theta}\|_2^2}$ and the upper hemisphere $\theta_{d+1} = \sqrt{1 - \|\boldsymbol{\theta}\|_2^2}$. As a result, the hyper-sphere is $\mathcal{S}^d = \{\tilde{\boldsymbol{\theta}} \in \mathbb{R}^{d+1} \mid \|\tilde{\boldsymbol{\theta}}\|_2 = 1\}$ and the domain of the unit ball $\mathcal{B}_0^d(1)$ is changed to \mathcal{S}^d by

$$T_{\mathcal{B} \rightarrow \mathcal{S}} : \mathcal{B} \mapsto \mathcal{S}_\pm^d, \quad \boldsymbol{\theta} \mapsto \tilde{\boldsymbol{\theta}} = \left(\boldsymbol{\theta}, \pm \sqrt{1 - \|\boldsymbol{\theta}\|_2^2} \right).$$

The map $T_{\mathcal{B} \rightarrow \mathcal{S}}$ changes the geometry of the problem. The original boundary ($\|\boldsymbol{\theta}\|_2 = 1$) becomes the equator of \mathcal{S}^d . A sampler moving freely on \mathcal{S}^d will implicitly “bounce off” this equator when mapped back to $\mathcal{B}_0^d(1)$, thus automatically respecting the constraint without explicit boundary checks.

The Hamiltonian dynamics are defined on the Riemannian manifold \mathcal{S}^d ([Lan et al., 2014](#)), endowed with the canonical spherical metric $\mathbf{G}_S = \mathbf{I}_d + \boldsymbol{\theta}\boldsymbol{\theta}^\top/(1 - \|\boldsymbol{\theta}\|_2^2)$. The Hamiltonian on the sphere is given by:

$$H^*(\tilde{\boldsymbol{\theta}}, \tilde{\mathbf{v}}) = U^*(\tilde{\boldsymbol{\theta}}) + K(\tilde{\mathbf{v}}) = U(\tilde{\boldsymbol{\theta}}) + \frac{1}{2}\tilde{\mathbf{v}}^\top \mathbf{I}_{d+1} \tilde{\mathbf{v}} = U(\boldsymbol{\theta}) + \frac{1}{2}\mathbf{v}^\top \mathbf{G}_S \mathbf{v}$$

where \mathbf{v} is sampled from the tangent space of $\mathcal{B}_0^d(1)$, and $\tilde{\mathbf{v}} = (\mathbf{v}, v_{d+1})$ is sampled from the tangent space of the unit sphere \mathcal{S}^d . The potential energy $U(\tilde{\boldsymbol{\theta}}) = U(\boldsymbol{\theta})$ and the kinetic energy $K(\tilde{\mathbf{v}}) = \frac{1}{2}\mathbf{v}^\top \mathbf{G}_S \mathbf{v} = \frac{1}{2}\|\tilde{\mathbf{v}}^2\|_2^2$. Given this Hamiltonian function defined on the sphere, the associated Hamiltonian dynamics are described by the following system of differential equations:

$$\begin{aligned} \dot{\tilde{\boldsymbol{\theta}}} &= \tilde{\mathbf{v}} \\ \dot{\tilde{\mathbf{v}}} &= -\|\tilde{\mathbf{v}}\|_2^2 \tilde{\boldsymbol{\theta}} - \mathcal{P}(\tilde{\boldsymbol{\theta}}) \nabla_{\tilde{\boldsymbol{\theta}}} U(\boldsymbol{\theta}) \end{aligned}$$

where the projection matrix $\mathcal{P}(\tilde{\boldsymbol{\theta}}) = \mathbf{I}_{d+1} - \tilde{\boldsymbol{\theta}}\tilde{\boldsymbol{\theta}}^\top$ maps the directional derivative $\nabla_{\tilde{\boldsymbol{\theta}}} U(\boldsymbol{\theta})$ onto the tangent space at $\tilde{\boldsymbol{\theta}}$. The velocity random variable $\tilde{\mathbf{v}} \sim \mathcal{N}(\mathbf{0}, \mathcal{P}(\tilde{\boldsymbol{\theta}}))$.

After obtaining the samples $\{\tilde{\boldsymbol{\theta}}\}$ using the above HMC, we discard the last component θ_{d+1} and obtain the samples $\{\boldsymbol{\theta}\}$ that automatically satisfy the constraint $\|\boldsymbol{\theta}\|_2 \leq 1$. The sign of θ_{d+1} does not affect the Monte Carlo estimates, but we need to adjust our estimates according to the change of variables theorem. We omit these details and summarize the SphHMC into the following Algorithm S2. [Lan and Kang \(2023\)](#) provided a comprehensive review of HMC and all constrained HMC, including SphHMC.

Three Benchmark Test Functions

Borehole function The function depends on eight inputs as follows [Surjanovic and Bingham \(n.d.\)](#):

$$f(\mathbf{x}) = \frac{2\pi T_u (H_u - H_l)}{\ln(r/r_w) \left(1 + \frac{2LT_u}{\ln(r/r_w)r_w^2 K_w} + \frac{T_u}{T_l} \right)} \quad (10)$$

Algorithm S2 Spherical Hamiltonian Monte Carlo

- 1: Given the step size ϵ and current $\boldsymbol{\theta}_{t-1}$, initialize $\tilde{\boldsymbol{\theta}}^{(0)}$ with $\tilde{\boldsymbol{\theta}}$ after transformation.
- 2: Sample a new velocity value $\tilde{\mathbf{v}}^{(0)} \sim \mathcal{N}(\mathbf{0}, \mathbf{I}_{d+1})$, and set $\tilde{\mathbf{v}}^{(0)} \leftarrow \tilde{\mathbf{v}}^{(0)} - \tilde{\boldsymbol{\theta}}^{(0)}(\tilde{\boldsymbol{\theta}}^{(0)})^\top \tilde{\mathbf{v}}^{(0)}$.
- 3: Calculate $H^*(\tilde{\boldsymbol{\theta}}^{(0)}, \tilde{\mathbf{v}}^{(0)}) = U(\boldsymbol{\theta}^{(0)}) + K(\tilde{\mathbf{v}}^{(0)})$.
- 4: **for** $l = 0$ to $L - 1$ **do**
- 5: $\tilde{\mathbf{v}}^{(l+\frac{1}{2})} = \tilde{\mathbf{v}}^{(l)} - \frac{\epsilon}{2} \mathcal{P}(\tilde{\boldsymbol{\theta}}^{(l)}) \nabla_{\tilde{\boldsymbol{\theta}}} U(\boldsymbol{\theta}^{(l)})$.
- 6: $\tilde{\boldsymbol{\theta}}^{(l+1)} = \tilde{\boldsymbol{\theta}}^{(l)} \cos(\|\tilde{\mathbf{v}}^{(l+\frac{1}{2})}\| \epsilon) + \frac{\tilde{\mathbf{v}}^{(l+\frac{1}{2})}}{\|\tilde{\mathbf{v}}^{(l+\frac{1}{2})}\|} \sin(\|\tilde{\mathbf{v}}^{(l+\frac{1}{2})}\| \epsilon)$
- 7: $\tilde{\mathbf{v}}^{(l+\frac{1}{2})} \leftarrow -\tilde{\boldsymbol{\theta}}^{(l)} \|\tilde{\mathbf{v}}^{(l+\frac{1}{2})}\| \sin(\|\tilde{\mathbf{v}}^{(l+\frac{1}{2})}\| \epsilon) + \tilde{\mathbf{v}}^{(l+\frac{1}{2})} \cos(\|\tilde{\mathbf{v}}^{(l+\frac{1}{2})}\| \epsilon)$
- 8: $\tilde{\mathbf{v}}^{(l+1)} = \tilde{\mathbf{v}}^{(l+\frac{1}{2})} - \frac{\epsilon}{2} \mathcal{P}(\tilde{\boldsymbol{\theta}}^{(l+1)}) \nabla_{\boldsymbol{\theta}} U(\boldsymbol{\theta}^{(l+1)})$
- 9: **end for**
- 10: Calculate $H^*(\tilde{\boldsymbol{\theta}}^{(L)}, \tilde{\mathbf{v}}^{(L)}) = U(\boldsymbol{\theta}^{(L)}) + K(\tilde{\mathbf{v}}^{(L)})$.
- 11: Compute the acceptance probability $\alpha = \min \left\{ 1, \exp(-H^*(\tilde{\boldsymbol{\theta}}^{(L)}, \tilde{\mathbf{v}}^{(L)}) + H^*(\tilde{\boldsymbol{\theta}}^{(0)}, \tilde{\mathbf{v}}^{(0)})) \right\}$
- 12: Accept or reject the proposal according to α for the next state $\tilde{\boldsymbol{\theta}}'$.
- 13: Apply the importance weights $|\frac{d\theta_B}{d\theta}|$ to the sample $\boldsymbol{\theta}$ based on $\tilde{\boldsymbol{\theta}}'$.

The following table S1 lists each input variable along with its corresponding parameter range and unit. ¹

Table S1: Borehole inputs and ranges

Symbol	Parameter	Range	Unit
r_w	radius of borehole	[0.05, 0.15]	m
r	radius of influence	[100, 50000]	m
T_u	transmissivity of upper aquifer	[63070, 115600]	m^2/yr
H_u	potentiometric head of upper aquifer	[990, 1110]	m
T_l	transmissivity of lower aquifer	[63.1, 116]	m^2/yr
H_l	potentiometric head of lower aquifer	[700, 820]	m
L	length of borehole	[1120, 1680]	m
K_w	hydraulic conductivity of borehole	[9855, 12045]	m/yr

OTL Circuit function. The function depends on six inputs as follows [Surjanovic and Bingham \(n.d.\)](#):

$$V_m(\mathbf{x}) = \frac{(V_{b1} + 0.74)\beta(R_{c2} + 9)}{\beta(R_{c2} + 9) + R_f} + \frac{11.35R_f}{\beta(R_{c2} + 9) + R_f} + \frac{0.74R_f\beta(R_{c2} + 9)}{(\beta(R_{c2} + 9) + R_f)R_{c1}} \quad (11)$$

where

$$V_{b1} = \frac{12R_{b2}}{R_{b1} + R_{b2}}.$$

The following table S2 lists each input variable along with its corresponding parameter range and unit. ²

¹Our mapping X_1, \dots, X_8 corresponds to $(r_w, r, T_u, H_u, T_l, H_l, L, K_w)$.

²Our mapping X_1, \dots, X_6 corresponds to $(R_{b1}, R_{b2}, R_f, R_{c1}, R_{c2}, \beta)$.

Table S2: OTL inputs and ranges

Symbol	Parameter	Range	Unit
R_{b1}	resistance $b1$	[50, 150]	K-Ohms
R_{b2}	resistance $b2$	[25, 70]	K-Ohms
R_f	resistance f	[0.5, 3]	K-Ohms
R_{c1}	resistance $c1$	[1.2, 2.5]	K-Ohms
R_{c2}	resistance $c2$	[0.25, 1.2]	K-Ohms
β	current gain	[50, 300]	Amperes

Piston function The function depends on seven inputs as follows [Surjanovic and Bingham \(n.d.\)](#):

$$\begin{aligned}
 C(\mathbf{x}) &= 2\pi \sqrt{\frac{M}{k + S^2 \frac{P_0 V_0}{T_0} \frac{T_a}{V^2}}}, \quad \text{where} \\
 V &= \frac{S}{2k} \left(\sqrt{A^2 + 4k \frac{P_0 V_0}{T_0} T_a} - A \right) \\
 A &= P_0 S + 19.62 M - \frac{k V_0}{S}
 \end{aligned} \tag{12}$$

The following table S3 lists each input variable along with its corresponding parameter range and unit. ³

Table S3: Piston inputs and ranges

Symbol	Parameter	Range	Unit
M	piston weight	[30, 60]	kg
S	piston surface area	[0.005, 0.020]	m^2
V_0	initial gas volume	[0.002, 0.010]	m^3
k	spring coefficient	[1000, 5000]	N/m
P_0	atmospheric pressure	[90000, 110000]	N/m^2
T_a	ambient temperature	[290, 296]	K
T_0	filling gas temperature	[340, 360]	K

Figures for Three Benchmark Examples

³Our mapping X_1, \dots, X_7 corresponds to $(M, S, V_0, k, P_0, T_a, T_0)$.

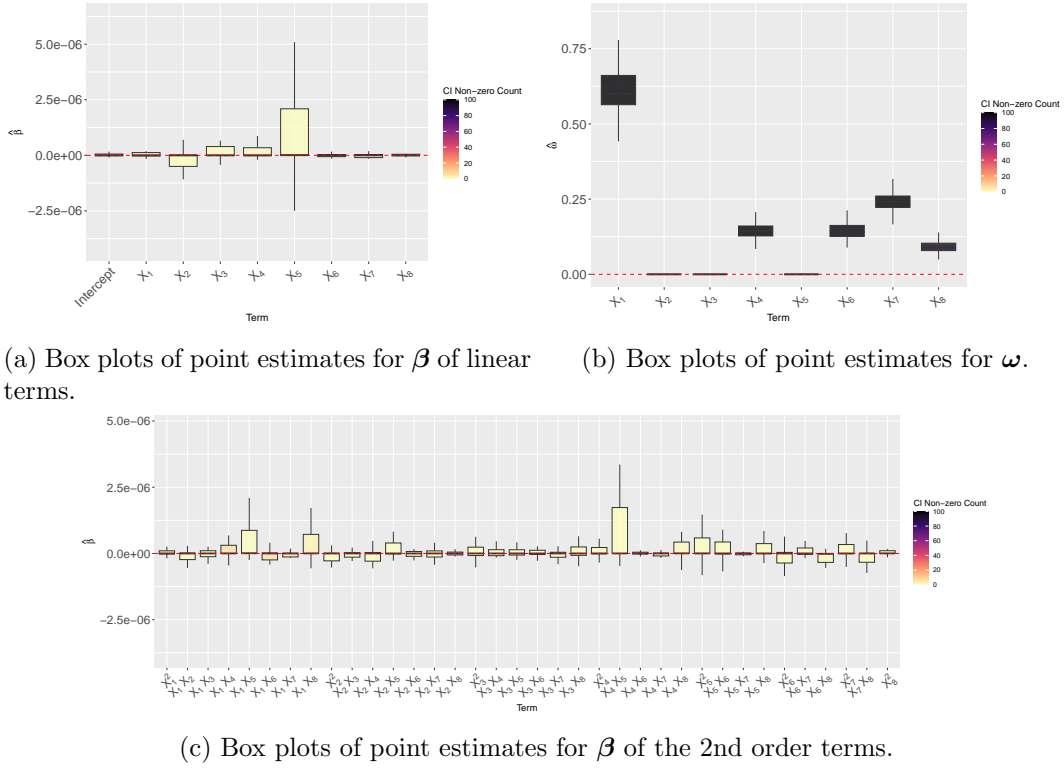


Figure S1: Box plot of point estimates for parameters for $n = 200$ for Borehole function.

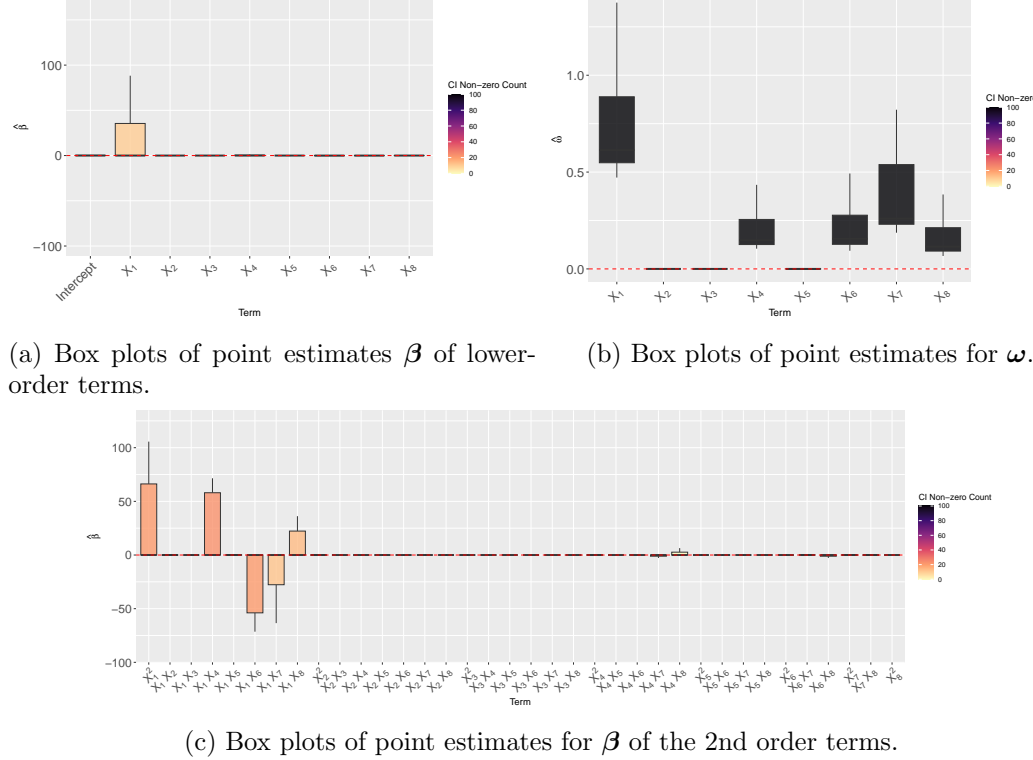
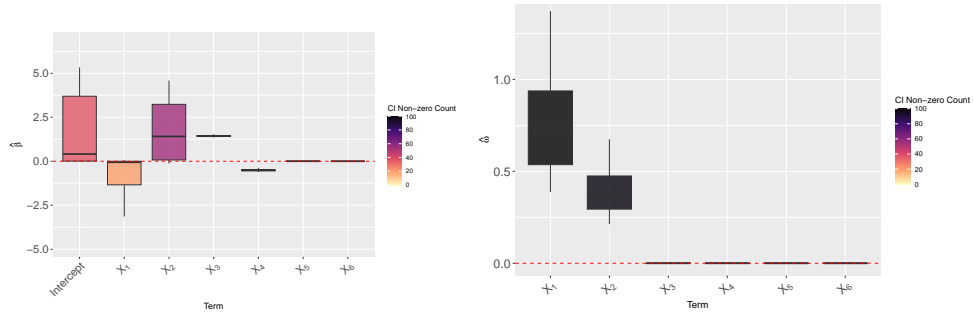
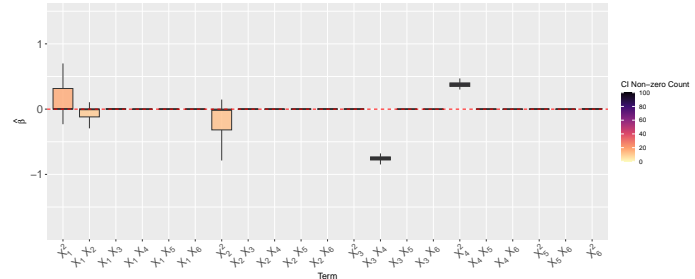


Figure S2: Box plot of point estimates for parameters for $n = 500$ for Borehole function.



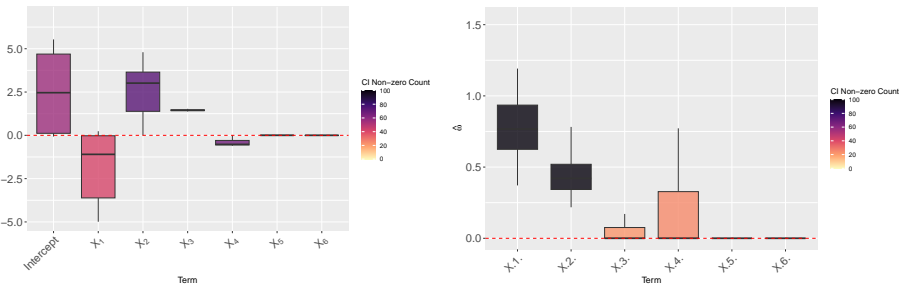
(a) Box plots of point estimates for β of lower-order terms.

(b) Box plots of point estimates for ω .



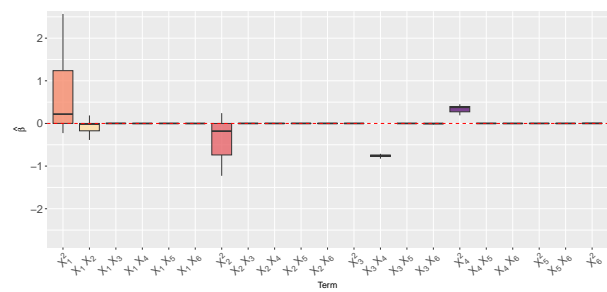
(c) Box plots of point estimates for β of the 2nd order terms.

Figure S3: Box plot of point estimates for parameters for $n = 200$ for OTL Circuit function.



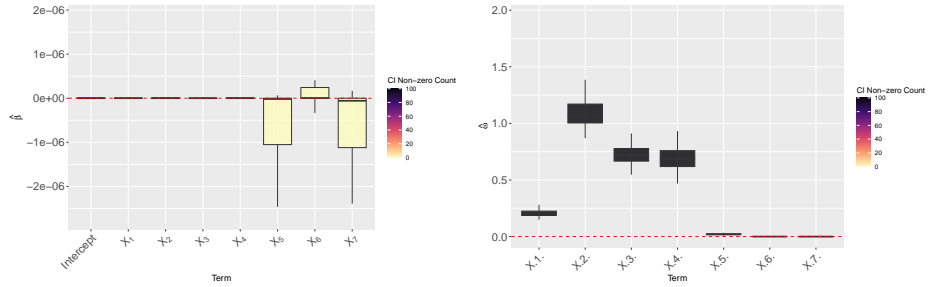
(a) Box plots of point estimates for β of lower-order terms.

(b) Box plots of point estimates for ω .

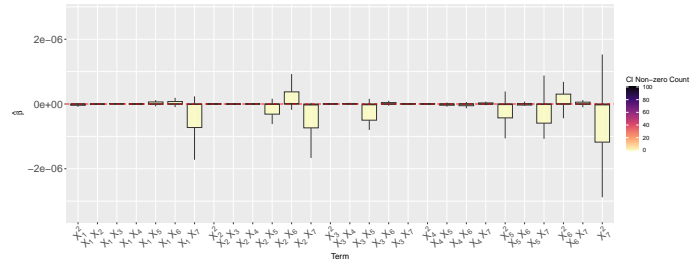


(c) Box plots of point estimates for β of the 2nd order terms.

Figure S4: Box plot of point estimates for parameters for $n = 500$ for OTL Circuit function.

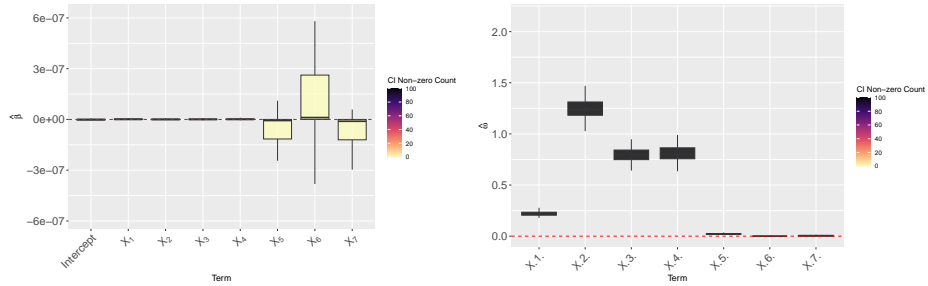


(a) Box plots of point estimates for β of lower-order terms. (b) Box plots of point estimates for ω .

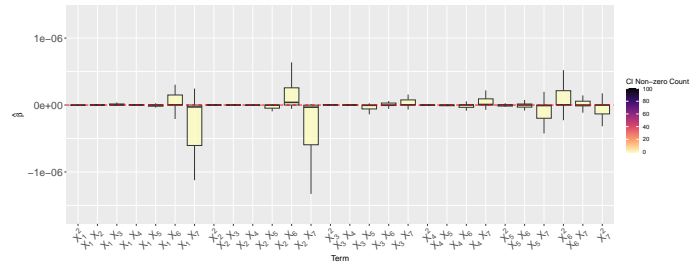


(c) Box plots of point estimates for β of the 2nd order terms.

Figure S5: Box plot of point estimates for parameters for $n = 200$ for Piston function.

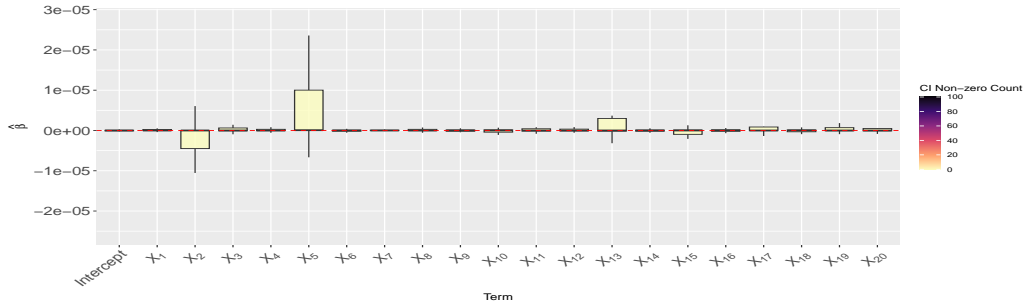


(a) Box plots of point estimates for β of lower-order terms. (b) Box plots of point estimates for ω .

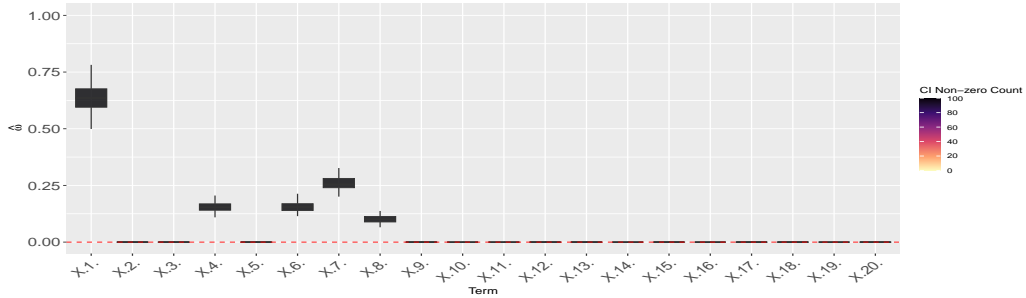


(c) Box plots of point estimates for β of the 2nd order terms.

Figure S6: Box plot of point estimates for parameters for $n = 500$ for Piston function.

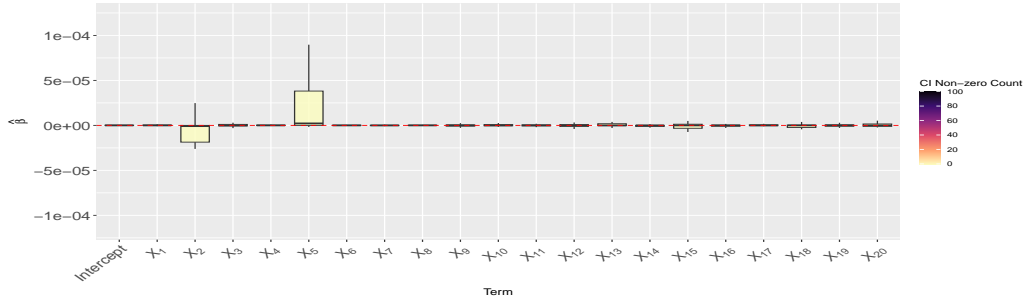


(a) Box plots of point estimates for β .

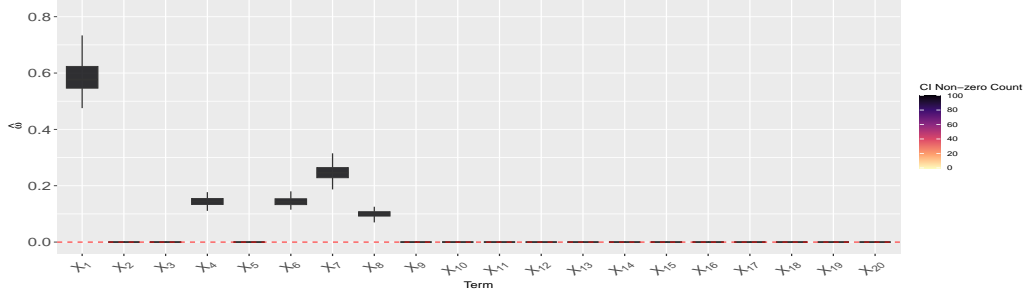


(b) Box plots of point estimates for ω .

Figure S7: Box plot of point estimates for parameters for the Borehole function with $n = 200$ and $d = 20$.

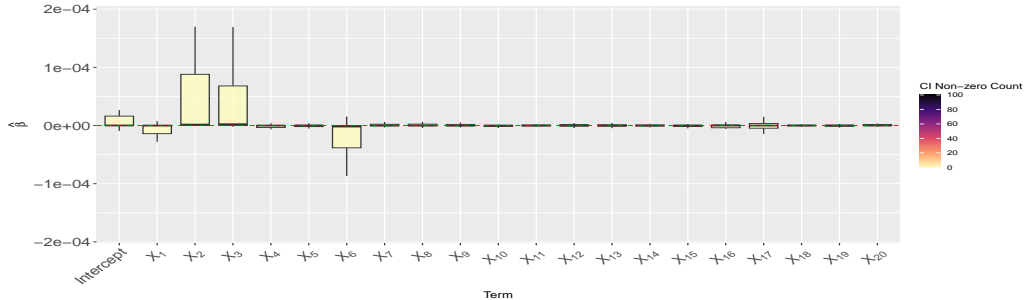


(a) Box plots of point estimates for β .

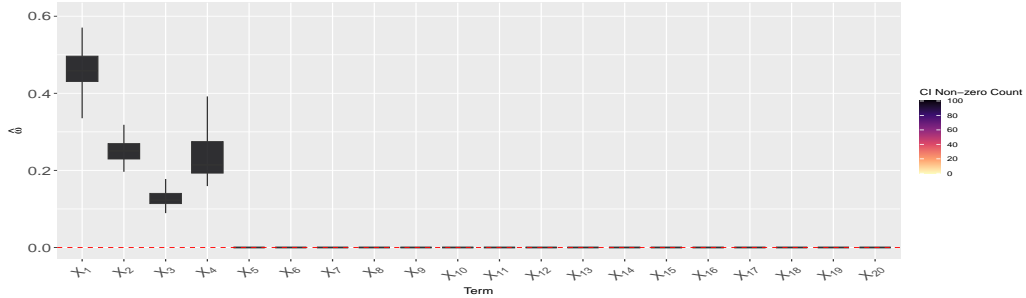


(b) Box plots of point estimates for ω .

Figure S8: Box plot of point estimates for parameters for the Borehole function with $n = 500$ and $d = 20$.

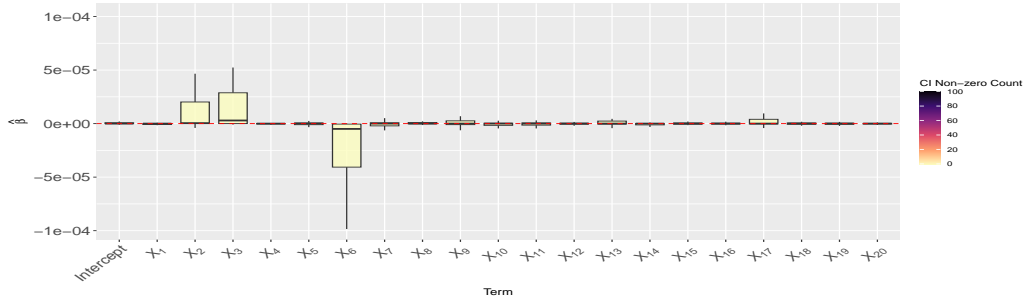


(a) Box plots of point estimates for β .

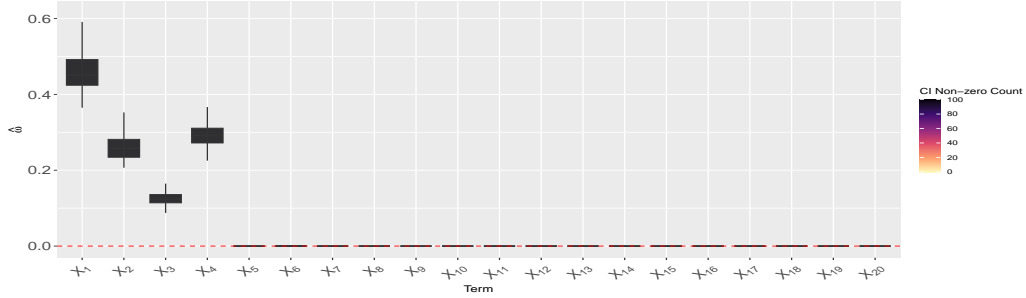


(b) Box plots of point estimates for ω .

Figure S9: Box plot of point estimates for parameters for the OTL Circuit function with $n = 200$ and $d = 20$.

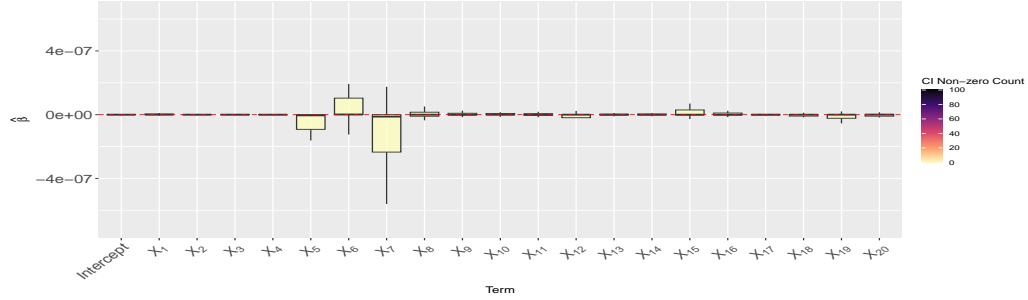


(a) Box plots of point estimates for β .

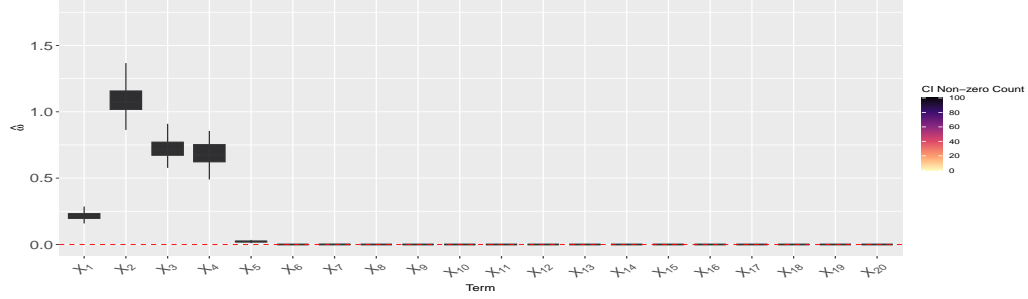


(b) Box plots of point estimates for ω .

Figure S10: Box plot of point estimates for parameters for the OTL Circuit function with $n = 500$ and $d = 20$.

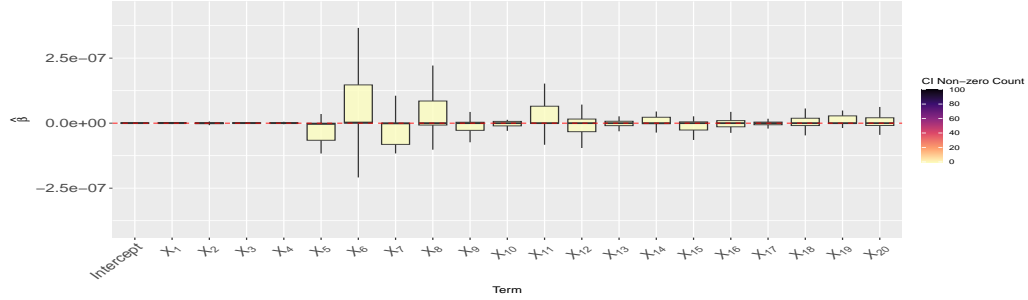


(a) Box plots of point estimates for β .

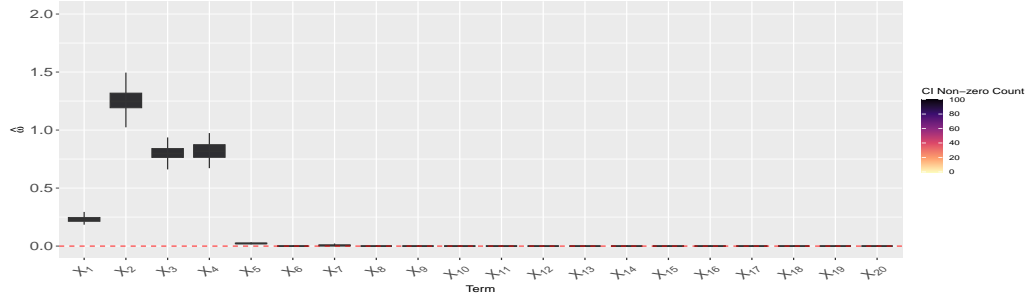


(b) Box plots of point estimates for ω .

Figure S11: Box plot of point estimates for parameters for the Piston function with $n = 200$ and $d = 20$.



(a) Box plots of point estimates for β .



(b) Box plots of point estimates for ω .

Figure S12: Box plot of point estimates for parameters for the Piston function with $n = 500$ and $d = 20$.

Derivation of Proposition 1

Given the prior as follows:

$$\begin{aligned}
p(\boldsymbol{\beta}|r_\beta) &\propto \mathbb{I}(\|\boldsymbol{\beta}\|_q \leq r_\beta), & \text{constrained non-informative prior,} \\
p(r_\beta) &\propto 1, & \text{non-informative prior,} \\
p(\boldsymbol{\omega}|r_\omega) &\propto \mathbb{I}(\|\boldsymbol{\omega}\|_q \leq r_\omega), & \text{constrained non-informative prior,} \\
p(r_\omega) &\propto 1, & \text{non-informative prior,} \\
\tau^2 &\sim \text{Inverse-}\chi^2(df_{\tau^2}), & \eta \sim \Gamma(a_\eta, b_\eta).
\end{aligned}$$

$$\begin{aligned}
p(\tau^2) &\propto (\tau^2)^{-\left(\frac{df_{\tau^2}}{2}+1\right)} \exp\left(-\frac{1}{2\tau^2}\right) \\
p(\eta) &\propto \eta^{a_\eta-1} \exp(-b_\eta \eta)
\end{aligned}$$

Given data, the sampling distribution is:

$$\begin{aligned}
\mathbf{y}_n | \boldsymbol{\beta}, \boldsymbol{\omega}, \tau^2, \eta &\sim \mathcal{MVN}_n(\mathbf{G}\boldsymbol{\beta}, \tau^2(\mathbf{K}_n + \eta\mathbf{I}_n)) \\
p(\mathbf{y}_n | \boldsymbol{\beta}, \boldsymbol{\omega}, \tau^2, \eta) &\propto (\tau^2)^{-\frac{n}{2}} \det(\mathbf{K}_n + \eta\mathbf{I}_n)^{-1/2} \\
&\times \exp\left(-\frac{1}{2\tau^2}(\mathbf{y}_n - \mathbf{G}\boldsymbol{\beta})^\top(\mathbf{K}_n + \eta\mathbf{I}_n)^{-1}(\mathbf{y}_n - \mathbf{G}\boldsymbol{\beta})\right)
\end{aligned} \tag{13}$$

Through the Bayes rule and (13), we have the following conditional posterior distributions for $\boldsymbol{\beta}$:

$$\begin{aligned}
p(\boldsymbol{\beta} | \mathbf{y}_n, \boldsymbol{\omega}, \tau^2, \eta) &\propto p(\mathbf{y}_n | \boldsymbol{\beta}, \boldsymbol{\omega}, \tau^2, \eta) p(\boldsymbol{\beta}) \\
&\propto (\tau^2)^{-\frac{n}{2}} \det(\mathbf{K}_n + \eta\mathbf{I}_n)^{-1/2} \exp\left(-\frac{1}{2\tau^2}(\mathbf{y}_n - \mathbf{G}\boldsymbol{\beta})^\top(\mathbf{K}_n + \eta\mathbf{I}_n)^{-1}(\mathbf{y}_n - \mathbf{G}\boldsymbol{\beta})\right) \\
&\times \mathbb{I}(\|\boldsymbol{\beta}\|_q \leq r_\beta) \\
&\propto \exp\left(-\frac{1}{2\tau^2}(\mathbf{y}_n - \mathbf{G}\boldsymbol{\beta})^\top(\mathbf{K}_n + \eta\mathbf{I}_n)^{-1}(\mathbf{y}_n - \mathbf{G}\boldsymbol{\beta})\right) \mathbb{I}(\|\boldsymbol{\beta}\|_q \leq r_\beta) \\
&\propto \exp\left(-\frac{1}{2\tau^2}(\mathbf{y}_n^\top(\mathbf{K}_n + \eta\mathbf{I}_n)^{-1}\mathbf{y}_n - 2\boldsymbol{\beta}^\top \mathbf{G}^\top(\mathbf{K}_n + \eta\mathbf{I}_n)^{-1}\mathbf{y}_n + \boldsymbol{\beta}^\top \mathbf{G}^\top(\mathbf{K}_n + \eta\mathbf{I}_n)^{-1}\mathbf{G}\boldsymbol{\beta})\right) \\
&\times \mathbb{I}(\|\boldsymbol{\beta}\|_q \leq r_\beta) \\
&\propto \exp\left(-\frac{1}{2\tau^2}(\boldsymbol{\beta}^\top \mathbf{G}^\top(\mathbf{K}_n + \eta\mathbf{I}_n)^{-1}\mathbf{G}\boldsymbol{\beta} - 2\boldsymbol{\beta}^\top \mathbf{G}^\top(\mathbf{K}_n + \eta\mathbf{I}_n)^{-1}\mathbf{y}_n)\right) \mathbb{I}(\|\boldsymbol{\beta}\|_q \leq r_\beta)
\end{aligned}$$

Following the above posterior density form, we have the following conditional posterior distribution for $\boldsymbol{\beta}$:

$$\begin{aligned}
\boldsymbol{\beta} | \mathbf{y}_n, \boldsymbol{\omega}, \tau^2, \eta &\sim \mathcal{MVN}_{px}\left(\hat{\boldsymbol{\beta}}_n, \boldsymbol{\Sigma}_{\boldsymbol{\beta}|n}\right) \mathbb{I}(\|\boldsymbol{\beta}\|_q \leq r_\beta) \\
\boldsymbol{\Sigma}_{\boldsymbol{\beta}|n} &= \tau^2(\mathbf{G}^\top(\mathbf{K}_n + \eta\mathbf{I}_n)^{-1}\mathbf{G})^{-1} \\
\hat{\boldsymbol{\beta}}_n &= \boldsymbol{\Sigma}_{\boldsymbol{\beta}|n} \frac{(\mathbf{G}^\top(\mathbf{K}_n + \eta\mathbf{I}_n)^{-1}\mathbf{y}_n)}{\tau^2} \\
&= (\mathbf{G}^\top(\mathbf{K}_n + \eta\mathbf{I}_n)^{-1}\mathbf{G})^{-1} \mathbf{G}^\top(\mathbf{K}_n + \eta\mathbf{I}_n)^{-1}\mathbf{y}_n
\end{aligned}$$

Since we have the mapping $\theta_{\beta_i} \mapsto \beta_i = r_{\beta} \cdot \text{sgn}(\theta_{\beta_i}) |\theta_{\beta_i}|^{2/q}$, the sampling distribution 13 can be re-expressed as:

$$\begin{aligned} p(\mathbf{y}_n | \boldsymbol{\theta}_{\beta}, r_{\beta}, \boldsymbol{\omega}, \tau^2, \eta) &\propto (\tau^2)^{-\frac{n}{2}} \det(\mathbf{K}_n + \eta \mathbf{I}_n)^{-1/2} \\ &\times \exp \left(-\frac{1}{2\tau^2} (\mathbf{y}_n - \mathbf{G}(\text{sgn}(\boldsymbol{\theta}_{\beta}) \circ |\boldsymbol{\theta}_{\beta}|^{\frac{2}{q}} r_{\beta}))^\top \right. \\ &\quad \left. \times (\mathbf{K}_n + \eta \mathbf{I}_n)^{-1} (\mathbf{y}_n - \mathbf{G}(\text{sgn}(\boldsymbol{\theta}_{\beta}) \circ |\boldsymbol{\theta}_{\beta}|^{\frac{2}{q}} r_{\beta})) \right) \end{aligned} \quad (14)$$

where \circ denotes the element-wise Hadamard product.

Through the Bayes rule and (14), we have the following conditional posterior distributions for r_{β} :

$$\begin{aligned} p(r_{\beta} | \mathbf{y}_n, \boldsymbol{\theta}_{\beta}, \boldsymbol{\omega}, \tau^2, \eta) &\propto p(\mathbf{y}_n | \boldsymbol{\theta}_{\beta}, r_{\beta}, \boldsymbol{\omega}, \tau^2, \eta) p(r_{\beta}) \\ &\propto \exp \left(-\frac{1}{2\tau^2} \left(\mathbf{y}_n - \mathbf{G}(r_{\beta} \text{sgn}(\boldsymbol{\theta}_{\beta}) \circ |\boldsymbol{\theta}_{\beta}|^{\frac{2}{q}}) \right)^\top (\mathbf{K}_n + \eta \mathbf{I}_n)^{-1} \right. \\ &\quad \left. \times \left(\mathbf{y}_n - \mathbf{G}(r_{\beta} \text{sgn}(\boldsymbol{\theta}_{\beta}) \circ |\boldsymbol{\theta}_{\beta}|^{\frac{2}{q}}) \right) \right) \\ -\log f(r_{\beta} | \mathbf{y}_n, \boldsymbol{\theta}_{\beta}, \boldsymbol{\omega}, \tau^2, \eta) &= \frac{1}{2\tau^2} \left(\mathbf{y}_n - \mathbf{G}(r_{\beta} \text{sgn}(\boldsymbol{\theta}_{\beta}) \circ |\boldsymbol{\theta}_{\beta}|^{\frac{2}{q}}) \right)^\top (\mathbf{K}_n + \eta \mathbf{I}_n)^{-1} \\ &\quad \times \left(\mathbf{y}_n - \mathbf{G}(r_{\beta} \text{sgn}(\boldsymbol{\theta}_{\beta}) \circ |\boldsymbol{\theta}_{\beta}|^{\frac{2}{q}}) \right) \end{aligned}$$

Through the Bayes rule and (13), we have the following conditional posterior distributions for $\boldsymbol{\omega}$:

$$\begin{aligned} p(\boldsymbol{\omega} | \mathbf{y}_n, \boldsymbol{\beta}, \tau^2, \eta) &\propto p(\mathbf{y}_n | \boldsymbol{\beta}, \boldsymbol{\omega}, \tau^2, \eta) p(\boldsymbol{\omega}) \\ &\propto \det(\mathbf{K}_n + \eta \mathbf{I}_n)^{-\frac{1}{2}} \exp \left(-\frac{1}{2\tau^2} (\mathbf{y}_n - \mathbf{G}\boldsymbol{\beta})^\top (\mathbf{K}_n + \eta \mathbf{I}_n)^{-1} (\mathbf{y}_n - \mathbf{G}\boldsymbol{\beta}) \right) \\ &\quad \times \mathbb{I}(\|\boldsymbol{\omega}\|_q \leq r_{\omega}) \\ \mathbf{K}_n(\mathbf{x}_i, \mathbf{x}_j; \boldsymbol{\omega}) &= \exp \left\{ -\sum_{k=1}^d \omega_k^2 (x_{ik} - x_{jk})^2 \right\} \end{aligned}$$

Omit the indicator function part for gradient calculation, we have:

$$\begin{aligned} -\log f(\boldsymbol{\omega} | \boldsymbol{\beta}, \tau^2, \eta, \mathbf{y}_n) &= \frac{1}{2} \log \det(\mathbf{K}_n + \eta \mathbf{I}_n) + \frac{1}{2\tau^2} (\mathbf{y}_n - \mathbf{G}\boldsymbol{\beta})^\top (\mathbf{K}_n + \eta \mathbf{I}_n)^{-1} (\mathbf{y}_n - \mathbf{G}\boldsymbol{\beta}) \\ \frac{\partial(-\log f(\boldsymbol{\omega} | \boldsymbol{\beta}, \tau^2, \eta, \mathbf{y}_n))}{\partial \omega_k} &= \frac{1}{2} \text{Tr}((\mathbf{K}_n + \eta \mathbf{I}_n)^{-1} \frac{\partial \mathbf{K}_n}{\partial \omega_k}) \\ &\quad - \frac{1}{2\tau^2} (\mathbf{y}_n - \mathbf{G}\boldsymbol{\beta})^\top (\mathbf{K}_n + \eta \mathbf{I}_n)^{-1} \frac{\partial \mathbf{K}_n}{\partial \omega_k} (\mathbf{K}_n + \eta \mathbf{I}_n)^{-1} (\mathbf{y}_n - \mathbf{G}\boldsymbol{\beta}) \\ \frac{\partial \mathbf{K}_n(\mathbf{x}_i, \mathbf{x}_j; \boldsymbol{\omega})}{\partial \omega_k} &= \mathbf{K}_n(\mathbf{x}_i, \mathbf{x}_j; \boldsymbol{\omega}) (-2\omega_k (x_{ik} - x_{jk})^2) \\ \nabla_{\boldsymbol{\omega}}(-\log f(\boldsymbol{\omega} | \boldsymbol{\beta}, \tau^2, \eta, \mathbf{y}_n)) &= \left(\frac{\partial}{\partial \omega_1}, \dots, \frac{\partial}{\partial \omega_d} \right) (-\log f(\boldsymbol{\omega} | \boldsymbol{\beta}, \tau^2, \eta, \mathbf{y}_n)) \end{aligned}$$

Since we have the mapping $\theta_{\omega_i} \mapsto \omega_i = r_{\omega} \cdot \text{sgn}(\theta_{\omega_i}) |\theta_{\omega_i}|^{2/q}$, the sampling distribution (13) can be re-expressed as:

$$\begin{aligned}
p(\mathbf{y}_n | \boldsymbol{\beta}, \boldsymbol{\theta}_{\omega}, r_{\omega}, \tau^2, \eta) &\propto (\tau^2)^{-\frac{n}{2}} \det(\mathbf{K}_n + \eta \mathbf{I}_n)^{-1/2} \exp \left(-\frac{1}{2\tau^2} (\mathbf{y}_n - \mathbf{G}\boldsymbol{\beta})^\top (\mathbf{K}_n + \eta \mathbf{I}_n)^{-1} (\mathbf{y}_n - \mathbf{G}\boldsymbol{\beta}) \right) \\
\text{where } \mathbf{K}_n(\mathbf{x}_i, \mathbf{x}_j; \boldsymbol{\omega}) &= \exp \left\{ -\sum_{k=1}^d \omega_k^2 (x_{ik} - x_{jk})^2 \right\} \\
&= \exp \left\{ -\sum_{k=1}^d (\text{sgn}(\theta_{\omega_k}) |\theta_{\omega_k}|^{\frac{2}{q}} r_{\omega})^2 (x_{ik} - x_{jk})^2 \right\} \\
&= \exp \left\{ -r_{\omega}^2 \sum_{k=1}^d |\theta_{\omega_k}|^{\frac{4}{q}} (x_{ik} - x_{jk})^2 \right\}
\end{aligned} \tag{15}$$

Through the Bayes rule and (15), we have the following conditional posterior distributions for r_{ω} :

$$\begin{aligned}
p(r_{\omega} | \mathbf{y}_n, \boldsymbol{\beta}, \boldsymbol{\theta}_{\omega}, \tau^2, \eta) &\propto p(\mathbf{y}_n | \boldsymbol{\beta}, \boldsymbol{\theta}_{\omega}, r_{\omega}, \tau^2, \eta) p(r_{\omega}) \\
&\propto \det(\mathbf{K}_n + \eta \mathbf{I}_n)^{-\frac{1}{2}} \exp \left(-\frac{1}{2\tau^2} (\mathbf{y}_n - \mathbf{G}\boldsymbol{\beta})^\top (\mathbf{K}_n + \eta \mathbf{I}_n)^{-1} (\mathbf{y}_n - \mathbf{G}\boldsymbol{\beta}) \right) \\
-\log f(r_{\omega} | \mathbf{y}_n, \boldsymbol{\beta}, \boldsymbol{\theta}_{\omega}, \tau^2, \eta) &= \frac{1}{2} \log \det(\mathbf{K}_n + \eta \mathbf{I}_n) + \frac{1}{2\tau^2} (\mathbf{y}_n - \mathbf{G}\boldsymbol{\beta})^\top (\mathbf{K}_n + \eta \mathbf{I}_n)^{-1} (\mathbf{y}_n - \mathbf{G}\boldsymbol{\beta}) \\
\mathbf{K}_n(\mathbf{x}_i, \mathbf{x}_j; \boldsymbol{\omega}) &= \exp \left\{ -r_{\omega}^2 \sum_{k=1}^d |\theta_{\omega_k}|^{\frac{4}{q}} (x_{ik} - x_{jk})^2 \right\}
\end{aligned}$$

Through the Bayes rule and (13), we have the following conditional posterior distributions for τ^2 :

$$\begin{aligned}
p(\tau^2 | \boldsymbol{\beta}, \boldsymbol{\omega}, \eta, \mathbf{y}_n) &\propto p(\tau^2) p(\mathbf{y}_n | \boldsymbol{\beta}, \boldsymbol{\omega}, \tau^2, \eta) \\
&\propto (\tau^2)^{-\left(\frac{df_{\tau^2}}{2} + 1\right)} \exp\left(-\frac{1}{2\tau^2}\right) (\tau^2)^{-\frac{n}{2}} \\
&\quad \times \exp \left(-\frac{1}{2\tau^2} (\mathbf{y}_n - \mathbf{G}\boldsymbol{\beta})^\top (\mathbf{K}_n + \eta \mathbf{I}_n)^{-1} (\mathbf{y}_n - \mathbf{G}\boldsymbol{\beta}) \right)
\end{aligned}$$

$$\text{Let } S_n^2 = (\mathbf{y}_n - \mathbf{G}\boldsymbol{\beta})^\top (\mathbf{K}_n + \eta \mathbf{I}_n)^{-1} (\mathbf{y}_n - \mathbf{G}\boldsymbol{\beta})$$

$$p(\tau^2 | \boldsymbol{\beta}, \boldsymbol{\omega}, \eta, \mathbf{y}_n) \propto (\tau^2)^{-\left(\frac{1}{2}(df_{\tau^2} + n) + 1\right)} \exp\left(-\frac{1 + S_n^2}{2\tau^2}\right)$$

$$\text{which implies } \tau^2 | \boldsymbol{\beta}, \boldsymbol{\omega}, \eta, \mathbf{y}_n \sim \text{Scaled Inverse-}\chi^2(df_{\tau^2} + n, \frac{1 + S_n^2}{df_{\tau^2} + n})$$

Through the Bayes rule and (13), we have the following conditional posterior distribu-

tions for η :

$$\begin{aligned}
p(\eta|\boldsymbol{\beta}, \boldsymbol{\omega}, \tau^2, \mathbf{y}_n) &\propto p(\eta)p(\mathbf{y}_n|\boldsymbol{\beta}, \boldsymbol{\omega}, \tau^2, \eta) \\
&\propto \eta^{a_\eta-1} e^{-b_\eta \eta} \det(\mathbf{K}_n + \eta \mathbf{I}_n)^{-\frac{1}{2}} \\
&\quad \times \exp\left(-\frac{1}{2\tau^2}(\mathbf{y}_n - \mathbf{G}\boldsymbol{\beta})^\top(\mathbf{K}_n + \eta \mathbf{I}_n)^{-1}(\mathbf{y}_n - \mathbf{G}\boldsymbol{\beta})\right) \\
-\log f(\eta|\boldsymbol{\beta}, \boldsymbol{\omega}, \tau^2, \mathbf{y}_n) &= (1 - a_\eta) \log \eta + b_\eta \eta + \frac{1}{2} \log \det(\mathbf{K}_n + \eta \mathbf{I}_n) \\
&\quad + \frac{1}{2\tau^2}(\mathbf{y}_n - \mathbf{G}\boldsymbol{\beta})^\top(\mathbf{K}_n + \eta \mathbf{I}_n)^{-1}(\mathbf{y}_n - \mathbf{G}\boldsymbol{\beta})
\end{aligned}$$

Derivation of Proposition 2

Given the prior as follows:

$$\begin{aligned}
\boldsymbol{\beta}|\nu_\beta^2 &\sim \mathcal{MVN}_p(\mathbf{0}, \nu_\beta^2 \mathbf{R}) \\
\nu_\beta^2 &\sim \text{Inverse-}\Gamma(a_\beta, b_\beta) \\
\omega_i|\nu_\omega^2 &\stackrel{\text{i.i.d.}}{\sim} \mathcal{N}(0, \nu_\omega^2), \text{ for } i = 1, \dots, d \\
\nu_\omega^2 &\sim \text{Inverse-}\Gamma(a_\omega, b_\omega) \\
\tau^2 &\sim \text{Inverse-}\chi^2(df_{\tau^2}) \\
\eta &\sim \Gamma(a_\eta, b_\eta)
\end{aligned}$$

Given data, the sampling distribution is the same as (13).

Through the Bayes rule and (13), we have the following conditional posterior distributions for $\boldsymbol{\beta}$:

$$\begin{aligned}
p(\boldsymbol{\beta}|\nu_\beta^2, \boldsymbol{\omega}, \nu_\omega^2, \tau^2, \eta, \mathbf{y}_n) &\propto p(\boldsymbol{\beta}|\nu_\beta^2)p(\mathbf{y}_n|\boldsymbol{\beta}, \nu_\beta^2, \boldsymbol{\omega}, \nu_\omega^2, \tau^2, \eta) \\
&\propto \det(\nu_\beta^2 \mathbf{R})^{-\frac{1}{2}} \exp\left(-\frac{1}{2}\boldsymbol{\beta}^\top(\nu_\beta^2 \mathbf{R})^{-1}\boldsymbol{\beta}\right) \\
&\quad \times \exp\left(-\frac{1}{2\tau^2}(\mathbf{y}_n - \mathbf{G}\boldsymbol{\beta})^\top(\mathbf{K}_n + \eta \mathbf{I}_n)^{-1}(\mathbf{y}_n - \mathbf{G}\boldsymbol{\beta})\right) \\
&\propto \exp\left(-\frac{1}{2}\boldsymbol{\beta}^\top(\nu_\beta^2 \mathbf{R})^{-1}\boldsymbol{\beta}\right) \exp\left(-\frac{1}{2\tau^2}(\mathbf{y}_n - \mathbf{G}\boldsymbol{\beta})^\top(\mathbf{K}_n + \eta \mathbf{I}_n)^{-1}(\mathbf{y}_n - \mathbf{G}\boldsymbol{\beta})\right)
\end{aligned}$$

Due to the conditional conjugacy or from the formula above (we can combine the terms in two exponential functions), we can find that the conditional posterior distribution of $\boldsymbol{\beta}$ is still a multivariate normal distribution.

$$\begin{aligned}
\boldsymbol{\beta}|\mathbf{y}_n, \nu_\beta^2, \boldsymbol{\omega}, \nu_\omega^2, \tau^2, \eta &\sim \mathcal{MVN}_p\left(\hat{\boldsymbol{\beta}}_n, \boldsymbol{\Sigma}_{\boldsymbol{\beta}|n}\right) \\
\boldsymbol{\Sigma}_{\boldsymbol{\beta}|n} &= \left[\frac{1}{\tau^2} \mathbf{G}^\top(\mathbf{K}_n + \eta \mathbf{I}_n)^{-1} \mathbf{G} + \frac{1}{\nu_\beta^2} \mathbf{R}^{-1}\right]^{-1} \\
\hat{\boldsymbol{\beta}}_n &= \boldsymbol{\Sigma}_{\boldsymbol{\beta}|n} \frac{(\mathbf{G}^\top(\mathbf{K}_n + \eta \mathbf{I}_n)^{-1} \mathbf{y}_n)}{\tau^2}
\end{aligned}$$

$$\begin{aligned}
p(\boldsymbol{\beta} | \mathbf{y}_n, \nu_{\beta}^2, \boldsymbol{\omega}, \nu_{\omega}^2, \tau^2, \eta) &\propto \exp\left(-\frac{1}{2}(\boldsymbol{\beta} - \hat{\boldsymbol{\beta}}_n)^{\top}(\boldsymbol{\Sigma}_{\boldsymbol{\beta}|n})^{-1}(\boldsymbol{\beta} - \hat{\boldsymbol{\beta}}_n)\right) \\
-\log f(\boldsymbol{\beta} | \mathbf{y}_n, \nu_{\beta}^2, \boldsymbol{\omega}, \nu_{\omega}^2, \tau^2, \eta) &= \frac{1}{2}(\boldsymbol{\beta} - \hat{\boldsymbol{\beta}}_n)^{\top}(\boldsymbol{\Sigma}_{\boldsymbol{\beta}|n})^{-1}(\boldsymbol{\beta} - \hat{\boldsymbol{\beta}}_n) \\
\nabla_{\boldsymbol{\beta}} - \log f(\boldsymbol{\beta} | \mathbf{y}_n, \nu_{\beta}^2, \boldsymbol{\omega}, \nu_{\omega}^2, \tau^2, \eta) &= (\boldsymbol{\Sigma}_{\boldsymbol{\beta}|n})^{-1}(\boldsymbol{\beta} - \hat{\boldsymbol{\beta}}_n)
\end{aligned}$$

Similarly, we can get the conditional posterior distribution of ν_{β}^2 as follows:

$$\begin{aligned}
p(\nu_{\beta}^2 | \boldsymbol{\beta}, \boldsymbol{\omega}, \nu_{\omega}^2, \tau^2, \eta, \mathbf{y}_n) &= \frac{p(\nu_{\beta}^2, \boldsymbol{\beta}, \boldsymbol{\omega}, \nu_{\omega}^2, \tau^2, \eta, \mathbf{y}_n)}{p(\boldsymbol{\beta}, \boldsymbol{\omega}, \nu_{\omega}^2, \tau^2, \eta, \mathbf{y}_n)} \\
&\propto p(\boldsymbol{\beta} | \nu_{\beta}^2) p(\nu_{\beta}^2) p(\mathbf{y}_n | \boldsymbol{\beta}, \nu_{\beta}^2, \boldsymbol{\omega}, \nu_{\omega}^2, \tau^2, \eta) \\
&\propto \det(\nu_{\beta}^2 \mathbf{R})^{-\frac{1}{2}} \exp\left(-\frac{1}{2} \boldsymbol{\beta}^{\top} (\nu_{\beta}^2 \mathbf{R})^{-1} \boldsymbol{\beta}\right) (\nu_{\beta}^2)^{-(a_{\beta}+1)} \exp\left(-\frac{b_{\beta}}{\nu_{\beta}^2}\right) \\
&\quad \times \exp\left(-\frac{1}{2\tau^2} (\mathbf{y}_n - \mathbf{G}\boldsymbol{\beta})^{\top} (\mathbf{K}_n + \eta \mathbf{I}_n)^{-1} (\mathbf{y}_n - \mathbf{G}\boldsymbol{\beta})\right) \\
&\propto \det(\mathbf{R})^{-\frac{1}{2}} (\nu_{\beta}^2)^{-(a_{\beta} + \frac{p}{2} + 1)} \exp\left(-\frac{1}{\nu_{\beta}^2} \left(\frac{1}{2} \boldsymbol{\beta}^{\top} \mathbf{R}^{-1} \boldsymbol{\beta} + b_{\beta}\right)\right) \\
\nu_{\beta}^2 | \boldsymbol{\beta}, \boldsymbol{\omega}, \tau^2, \eta, \mathbf{y}_n &\sim \text{Inverse-}\Gamma\left(a_{\beta} + \frac{p}{2}, \frac{1}{2} \boldsymbol{\beta}^{\top} \mathbf{R}^{-1} \boldsymbol{\beta} + b_{\beta}\right)
\end{aligned}$$

If R is identity matrix, then

$$\begin{aligned}
p(\nu_{\beta}^2 | \boldsymbol{\beta}, \boldsymbol{\omega}, \nu_{\omega}^2, \tau^2, \eta, \mathbf{y}_n) &\propto (\nu_{\beta}^2)^{-(a_{\beta} + \frac{p}{2} + 1)} \exp\left(-\frac{1}{\nu_{\beta}^2} \left(\frac{1}{2} \boldsymbol{\beta}^{\top} \boldsymbol{\beta} + b_{\beta}\right)\right) \\
\nu_{\beta}^2 | \boldsymbol{\beta}, \boldsymbol{\omega}, \nu_{\omega}^2, \tau^2, \eta, \mathbf{y}_n &\sim \text{Inverse-}\Gamma\left(a_{\beta} + \frac{p}{2}, \frac{1}{2} \boldsymbol{\beta}^{\top} \boldsymbol{\beta} + b_{\beta}\right)
\end{aligned}$$

We can get the conditional posterior distribution of $\boldsymbol{\omega}$ as follows:

$$\begin{aligned}
p(\boldsymbol{\omega}|\boldsymbol{\beta}, \nu_{\beta}^2, \nu_{\omega}^2, \tau^2, \eta, \mathbf{y}_n) &\propto \left(\prod_{i=1}^d p(\omega_i|\nu_{\omega}^2) \right) p(\mathbf{y}_n|\boldsymbol{\beta}, \nu_{\beta}^2, \boldsymbol{\omega}, \nu_{\omega}^2, \tau^2, \eta) \\
p(\boldsymbol{\omega}|\boldsymbol{\beta}, \nu_{\beta}^2, \nu_{\omega}^2, \tau^2, \eta, \mathbf{y}_n) &\propto \left(\prod_{i=1}^d (\nu_{\omega}^2)^{-\frac{1}{2}} \exp\left(-\frac{\omega_i^2}{2\nu_{\omega}^2}\right) \right) \det(\mathbf{K}_n + \eta\mathbf{I}_n)^{-\frac{1}{2}} \\
&\quad \times \exp\left(-\frac{1}{2\tau^2}(\mathbf{y}_n - \mathbf{G}\boldsymbol{\beta})^\top(\mathbf{K}_n + \eta\mathbf{I}_n)^{-1}(\mathbf{y}_n - \mathbf{G}\boldsymbol{\beta})\right) \\
&\propto \left(\prod_{i=1}^d \exp\left(-\frac{\omega_i^2}{2\nu_{\omega}^2}\right) \right) \det(\mathbf{K}_n + \eta\mathbf{I}_n)^{-\frac{1}{2}} \\
&\quad \times \exp\left(-\frac{1}{2\tau^2}(\mathbf{y}_n - \mathbf{G}\boldsymbol{\beta})^\top(\mathbf{K}_n + \eta\mathbf{I}_n)^{-1}(\mathbf{y}_n - \mathbf{G}\boldsymbol{\beta})\right) \\
-\log f(\boldsymbol{\omega}|\boldsymbol{\beta}, \nu_{\beta}^2, \nu_{\omega}^2, \tau^2, \eta, \mathbf{y}_n) &= \sum_{i=1}^d \left(\frac{\omega_i^2}{2\nu_{\omega}^2} \right) + \frac{1}{2} \log \det(\mathbf{K}_n + \eta\mathbf{I}_n) \\
&\quad + \frac{1}{2\tau^2}(\mathbf{y}_n - \mathbf{G}\boldsymbol{\beta})^\top(\mathbf{K}_n + \eta\mathbf{I}_n)^{-1}(\mathbf{y}_n - \mathbf{G}\boldsymbol{\beta}) \\
\frac{\partial(-\log f(\boldsymbol{\omega}|\boldsymbol{\beta}, \nu_{\beta}^2, \nu_{\omega}^2, \tau^2, \eta, \mathbf{y}_n))}{\partial\omega_k} &= \frac{\omega_k}{\nu_{\omega}^2} + \frac{1}{2} \text{Tr}((\mathbf{K}_n + \eta\mathbf{I}_n)^{-1} \frac{\partial\mathbf{K}_n}{\partial\omega_k}) \\
&\quad - \frac{1}{2\tau^2}(\mathbf{y}_n - \mathbf{G}\boldsymbol{\beta})^\top(\mathbf{K}_n + \eta\mathbf{I}_n)^{-1} \frac{\partial\mathbf{K}_n}{\partial\omega_k} (\mathbf{K}_n + \eta\mathbf{I}_n)^{-1}(\mathbf{y}_n - \mathbf{G}\boldsymbol{\beta}) \\
\nabla_{\boldsymbol{\omega}}(-\log f(\boldsymbol{\omega}|\boldsymbol{\beta}, \nu_{\beta}^2, \nu_{\omega}^2, \tau^2, \eta, \mathbf{y}_n)) &= \left(\frac{\partial}{\partial\omega_1}, \dots, \frac{\partial}{\partial\omega_d} \right) (-\log f(\boldsymbol{\omega}|\boldsymbol{\beta}, \nu_{\beta}^2, \nu_{\omega}^2, \tau^2, \eta, \mathbf{y}_n))
\end{aligned}$$

Considering the specific element of the kernel matrix \mathbf{K}_n , we have

$$\begin{aligned}
\mathbf{K}_n(\mathbf{x}_i, \mathbf{x}_j; \boldsymbol{\omega}) &= \exp\left\{-\sum_{k=1}^d \omega_k^2 (x_{ik} - x_{jk})^2\right\} \\
\frac{\partial\mathbf{K}_n(\mathbf{x}_i, \mathbf{x}_j; \boldsymbol{\omega})}{\partial\omega_k} &= \mathbf{K}_n(\mathbf{x}_i, \mathbf{x}_j; \boldsymbol{\omega}) (-2\omega_k(x_{ik} - x_{jk})^2)
\end{aligned}$$

Then we can get the conditional posterior distribution of ν_{ω}^2 as follows:

$$\begin{aligned}
p(\nu_{\omega}^2|\boldsymbol{\beta}, \nu_{\beta}^2, \boldsymbol{\omega}, \tau^2, \eta, \mathbf{y}_n) &= \frac{p(\nu_{\omega}^2, \boldsymbol{\beta}, \nu_{\beta}^2, \boldsymbol{\omega}, \tau^2, \eta, \mathbf{y}_n)}{p(\boldsymbol{\beta}, \nu_{\beta}^2, \boldsymbol{\omega}, \tau^2, \eta, \mathbf{y}_n)} \\
&\propto p(\boldsymbol{\omega}|\nu_{\omega}^2) p(\nu_{\omega}^2) p(\mathbf{y}_n|\boldsymbol{\beta}, \nu_{\beta}^2, \boldsymbol{\omega}, \nu_{\omega}^2, \tau^2, \eta) \\
&\propto \left(\prod_{i=1}^d (\nu_{\omega}^2)^{-\frac{1}{2}} \exp\left(-\frac{\omega_i^2}{2\nu_{\omega}^2}\right) \right) (\nu_{\omega}^2)^{-(a_{\omega}+1)} \exp\left(-\frac{b_{\omega}}{\nu_{\omega}^2}\right) \\
&\quad \det(\mathbf{K}_n + \eta\mathbf{I}_n)^{-\frac{1}{2}} \exp\left(-\frac{1}{2\tau^2}(\mathbf{y}_n - \mathbf{G}\boldsymbol{\beta})^\top(\mathbf{K}_n + \eta\mathbf{I}_n)^{-1}(\mathbf{y}_n - \mathbf{G}\boldsymbol{\beta})\right) \\
&\propto (\nu_{\omega}^2)^{-(a_{\omega}+\frac{d}{2}+1)} \exp\left(-\frac{1}{\nu_{\omega}^2} \left(\frac{1}{2} \sum_{i=1}^d \omega_i^2 + b_{\omega} \right) \right)
\end{aligned}$$

$$\nu_\omega^2 | \boldsymbol{\beta}, \nu_\beta^2, \boldsymbol{\omega}, \tau^2, \eta, \mathbf{y}_n \sim \text{Inverse-}\Gamma \left(a_\omega + \frac{d}{2}, \frac{1}{2} \sum_{i=1}^d \omega_i^2 + b_\omega \right)$$

Similarly, we can get the conditional posterior distribution of τ^2 as follows:

$$\begin{aligned} p(\tau^2 | \boldsymbol{\beta}, \nu_\beta^2, \boldsymbol{\omega}, \nu_\omega^2, \eta, \mathbf{y}_n) &\propto p(\tau^2) p(\mathbf{y}_n | \boldsymbol{\beta}, \nu_\beta^2, \boldsymbol{\omega}, \nu_\omega^2, \tau^2, \eta) \\ &\propto (\tau^2)^{-(\frac{df_{\tau^2}}{2} + 1)} \exp(-\frac{1}{2\tau^2})(\tau^2)^{-\frac{n}{2}} \\ &\quad \times \exp \left(-\frac{1}{2\tau^2} (\mathbf{y}_n - \mathbf{G}\boldsymbol{\beta})^\top (\mathbf{K}_n + \eta \mathbf{I}_n)^{-1} (\mathbf{y}_n - \mathbf{G}\boldsymbol{\beta}) \right) \end{aligned}$$

Let $S_n^2 = (\mathbf{y}_n - \mathbf{G}\boldsymbol{\beta})^\top (\mathbf{K}_n + \eta \mathbf{I}_n)^{-1} (\mathbf{y}_n - \mathbf{G}\boldsymbol{\beta})$, we have

$$\begin{aligned} p(\tau^2 | \boldsymbol{\beta}, \nu_\beta^2, \boldsymbol{\omega}, \nu_\omega^2, \eta, \mathbf{y}_n) &\propto (\tau^2)^{-(\frac{1}{2}(df_{\tau^2} + n) + 1)} \exp(-\frac{1 + S_n^2}{2\tau^2}) \\ \text{which implies } \tau^2 | \boldsymbol{\beta}, \nu_\beta^2, \boldsymbol{\omega}, \nu_\omega^2, \eta, \mathbf{y}_n &\sim \text{Scaled Inverse-}\chi^2(df_{\tau^2} + n, \frac{1 + S_n^2}{df_{\tau^2} + n}) \end{aligned}$$

Then we can get the conditional posterior distribution of η as follows:

$$\begin{aligned} p(\eta | \boldsymbol{\beta}, \nu_\beta^2, \boldsymbol{\omega}, \nu_\omega^2, \tau^2, \mathbf{y}_n) &\propto p(\eta) p(\mathbf{y}_n | \boldsymbol{\beta}, \nu_\beta^2, \boldsymbol{\omega}, \nu_\omega^2, \tau^2, \eta) \\ &\propto \eta^{a_\eta - 1} e^{-b_\eta \eta} \det(\mathbf{K}_n + \eta \mathbf{I}_n)^{-\frac{1}{2}} \\ &\quad \times \exp \left(-\frac{1}{2\tau^2} (\mathbf{y}_n - \mathbf{G}\boldsymbol{\beta})^\top (\mathbf{K}_n + \eta \mathbf{I}_n)^{-1} (\mathbf{y}_n - \mathbf{G}\boldsymbol{\beta}) \right) \\ -\log f(\eta | \boldsymbol{\beta}, \nu_\beta^2, \boldsymbol{\omega}, \nu_\omega^2, \tau^2, \mathbf{y}_n) &= (1 - a_\eta) \log \eta + b_\eta \eta + \frac{1}{2} \log \det(\mathbf{K}_n + \eta \mathbf{I}_n) \\ &\quad + \frac{1}{2\tau^2} (\mathbf{y}_n - \mathbf{G}\boldsymbol{\beta})^\top (\mathbf{K}_n + \eta \mathbf{I}_n)^{-1} (\mathbf{y}_n - \mathbf{G}\boldsymbol{\beta}) \end{aligned}$$